Published in final edited form as:

Sci Immunol. 2021 September 17; 6(63): eabf6723. doi:10.1126/sciimmunol.abf6723.

Combined immunodeficiency with autoimmunity caused by a homozygous missense mutation in inhibitor of nuclear factor κB kinase alpha (IKKα)

Wayne Bainter[1,†], **Vassilios Lougaris**[2,†], **Jacqueline G. Wallace**[1,†], **Yousef Badran**[1], **Rodrigo Hoyos-Bachiloglu**[1], **Zachary Peters**[1], **Hazel Wilkie**[1], **Mrinmoy Das**[1], **Erin Janssen**[1], **Abdallah Beano**[1], **Khaoula Ben Farhat**[1], **Christy Kam**[1], **Luisa Bercich**[3], **Paolo Incardona**[3], **Vincenzo Villanacci**[3], **Maria Pia Bondioni**[4], **Antonella Meini**[2], **Manuela Baronio**[2], **Phammela Abarzua**[5], **Silvia Parolini**[2], **Giovanna Tabellini**[2], **Stefano Maio**[6], **Birgitta Schmidt**[7], **Jeffrey D. Goldsmith**[7], **George Murphy**[5], **Georg Hollander**[6,8,9,‡], **Alessandro Plebani**[2,‡], **Janet Chou**[1,‡], **Raif S. Geha**[1,*,‡]

[1]Division of Immunology, Boston Children's Hospital, Harvard Medical School, Boston, MA, USA.

[2]Pediatrics Clinic, Institute for Molecular Medicine A. Nocivelli, Department of Clinical and Experimental Sciences, University of Brescia, ASST-Spedali Civili of Brescia, Brescia, Italy.

[3]Department of Pathology, University of Brescia, ASST Spedali Civili of Brescia, Brescia, Italy.

[4]Department of Pediatric Radiology, University of Brescia, ASST Spedali Civili of Brescia, Brescia, Italy.

[5]Department of Dermatology, Brigham and Women's Hospital, Harvard Medical School, Boston, MA, USA.

[6]Department of Paediatrics, the Weatherall Institute of Molecular Medicine, University of Oxford, Oxford, UK.

[7]Department of Pathology, Boston Children's Hospital, Harvard Medical School, Boston, MA, USA.

[8]Paediatric Immunology, Department of Biomedicine, University of Basel, University Children's Hospital Basel, Basel, Switzerland.

*Corresponding author. raif.geha@childrens.harvard.edu.

Author contributions: W.B., J.G.W., Y.B., R.H.-B., Z.P., H.W., M.D., E.J., A.B., K.B.F., C.K., P.A., S.P., G.T., and S.M. performed the experiments. V.L., L.B., P.I., V.V., M.P.B., A.M., M.B., and A.P. collected and analyzed the clinical data. W.B., J.G.W., B.S., J.D.G., G.M., G.H., J.C., and R.S.G. analyzed the data and wrote the manuscript.

†These authors contributed equally to this work.

‡These authors contributed equally to this work as senior co-authors.

SUPPLEMENTARY MATERIALS

www.science.org/doi/10.1126/sciimmunol.abf6723

Figs. S1 to S9

Table S1

Data file S1

View/request a protocol for this paper from Bio-protocol.

Competing interests: The authors declare that they have no competing interests.

[9]Department of Biosystems Science and Engineering, ETH Zurich, Basel, Switzerland.

Abstract

Inhibitor of nuclear factor kappa B kinase alpha (IKKα) is critical for p100/NF-κB2 phosphorylation and processing into p52 and activation of the noncanonical NF-κB pathway. A patient with recurrent infections, skeletal abnormalities, absent secondary lymphoid structures, reduced B cell numbers, hypogammaglobulinemia, and lymphocytic infiltration of intestine and liver was found to have a homozygous p.Y580C mutation in the helix-loop-helix domain of IKKα. The mutation preserves IKKα kinase activity but abolishes the interaction of IKKα with its activator NF-κB–inducing kinase and impairs lymphotoxin-β–driven p100/NF-κB2 processing and *VCAM1* expression. Homozygous $IKK\alpha^{Y580C/Y580C}$ mutant mice phenocopy the patient findings; lack marginal zone B cells, germinal centers, and antigen-specific T cell response to cutaneous immunization; have impaired *Il17a* expression; and are susceptible to cutaneous *Staphylococcus aureus* infection. In addition, these mice demonstrate a severe reduction in medullary thymic epithelial cells, impaired thymocyte negative selection, a restricted TCRVβ repertoire, a selective expansion of potentially autoreactive T cell clones, a decreased frequency of regulatory T cells, and infiltration of liver, pancreas, and lung by activated T cells coinciding with organ damage. Hence, this study identifies IKKα deficiency as a previously undescribed cause of primary immunodeficiency with associated autoimmunity.

INTRODUCTION

The nuclear factor κB (NF-κB) family of transcription factors is important for the proper development and function of both hematopoietic and stromal cells (1). It includes five members: RelA (p65), RelB, c-Rel, NF-κB1 (p105), and NF-κB2 (p100) (2), which participate in either canonical or noncanonical NF-κB activation. The canonical, or classical, pathway of NF-κB activation results in the rapid expression of inflammatory cytokines, chemokines, and adhesion molecules after ligation of Toll-like receptors, ectodysplasin A receptor, tumor necrosis factor–α (TNF-α), and interleukin-1 (IL-1) receptor family members, CD40, and T and B cell antigen receptors (3). Ligation of these receptors activates the inhibitor of NF-κB kinase (IKK) complex composed of the catalytic α and β subunits (designated IKKα and IKKβ, respectively) and the regulatory γ subunit IKKγ [designated nuclear factor-kappa B essential modulator (NEMO)]. The IKK complex phosphorylates IκBα, thus marking it for polyubiquitination and subsequent degradation by the 26*S* proteasome (4). The degradation of IκBα liberates p50/p65 dimers to translocate to the nucleus and activate the transcription of genes necessary for the inflammatory response (4). IKKβ and IKKγ are essential for canonical NF-κB activation, whereas IKKα is dispensable (5).

In contrast to canonical NF-κB activation, noncanonical activation of NF-κB signaling requires hours to cause the expression of genes that include chemokines and adhesion molecules involved in lymphorganogenesis, cell activation and survival, and tissue remodeling. Activation of the noncanonical NF-κB pathway occurs after ligation of surface receptors that include the lymphotoxin beta receptor (LTβR), B cell–activating factor receptor (BAFF-R), CD40, and receptor activator of NF-κB (RANK). Ligation of

these receptors stabilizes the NF-κB–inducing kinase (NIK), which activates IKKα. NIK-activated IKKα docks to and phosphorylates p100 (NF-κB2), which is in the cytoplasm complexed to RelB (6). Phosphorylated p100 undergoes polyubiquitination and proteasome processing into p52, allowing the p52:RelB dimer to translocate to the nucleus and activate the transcription of genes involved in the formation of secondary lymphoid organs (SLO), thymic epithelial cell (TEC) differentiation, B cell survival and activation, and bone matrix formation (7–13). IKKα is essential for noncanonical NF-κB activation, whereas IKKβ is dispensable (14).

Mutations in all five NF-κB family members, as well as in the IKK complex members IKKβ and IKKγ and in NIK, have been associated with immunodeficiency and/or immune dysregulation (7, 15–22). The only mutations known to date in IKKα are nonsense mutations that when homozygous cause cocoon syndrome, an embryonic lethal encasement syndrome (23). The phenotype of this syndrome closely resembles that of IKKα null mice, which die at birth with failed epidermal keratinization, hypoplastic limbs, and other skeletal abnormalities (24–27).

We present a patient with combined immunodeficiency and an autosomal recessive Y580C missense mutation in IKKα. While maintaining intrinsic kinase function, the mutation abolishes IKKα interaction with NIK as well as ligand-induced p100 processing and noncanonical NF-κB activation. IKKα$^{Y580C/Y580C}$ mice generated by CRISPR-Cas9 gene editing demonstrate a lack of SLO, impaired T and B cell function, virtual absence of mTECs, impaired thymocyte negative selection of CD4$^+$ cells, restricted T cell receptor variable beta chain (TCRVβ) repertoire, expansion of potentially autoreactive T cell clones, and autoimmunity marked by mononuclear organ infiltration and damage.

RESULTS

Patient characteristics

The patient, a daughter of consanguineous Italian parents, presented at 2 years of age with a history of recurrent pneumonias and failure to thrive (weight and height below third percentile). The patient lacked secondary lymphoid tissues such as palpable lymph nodes (LNs) and the Waldeyer’s ring. Later in life, she was found to have skeletal abnormalities including incomplete fusions of bones in the sternum and sacrum and absent ossification of the last segment of the sternum body and xiphoid process (Fig. 1A). Laboratory evaluation at presentation revealed pan-hypogammaglobulinemia and B cell lymphopenia (Table 1). The numbers of circulating CD4$^+$, CD8$^+$ T cells, and CD3$^-$CD56$^+$ natural killer (NK) cells were normal, but there was a preponderance of CD56^{bright} immature NK cells (Table 1). With age, the patient’s T cell and NK cell counts decreased, and the B cell lymphopenia worsened (Table 1 and fig. S1A). Proliferation of peripheral blood mononuclear cells (PBMCs) in response to phytohemagglutinin and anti-CD3 stimulation was normal at age 2. NK cell function examined at age 16 showed defective proliferation to IL-2 and impaired interferon-γ (IFN-γ) secretion after stimulation with IL-12 + IL-18 (fig. S2, A and B). The patient was treated with intravenous immunoglobulin (IVIG) but continued to suffer from recurrent sinopulmonary infections and over time developed bronchiectasis. She also suffered from recurrent skin infections including impetigo caused by *Staphylococcus*

aureus, mucocutaneous candidiasis with fungal organisms detected by periodic acid–Schiff staining (Fig. 1B, top), and epidermodysplasia verruciformis with characteristic histological changes and positive immune staining for human papilloma virus (HPV) (Fig. 1B, bottom). Nonlesional skin had increased epidermal thickness and hyperkeratosis, increased numbers of proliferating $Ki67^+$ cells in the basal and suprabasal cell layers of the epidermis, and mononuclear cell infiltration of the dermis (Fig. 1C). The patient developed chronic diarrhea starting at age 13. *Giardia lamblia* were recovered from stools on two occasions at ages 13 and 16, and *Salmonella enteritidis* was found on four occasions at ages 14, 17, 19, and 20. Biopsies of the duodenum and colon taken at age 15, when stool cultures were negative for pathogenic bacteria and viruses, showed mild villous atrophy, increased infiltration with T cells in the duodenum, and increased numbers of apoptotic basal crypt epithelial cells in the colon (Fig. 1, D and E), suggestive of autoimmune enteropathy. After age 12, the patient developed progressive elevation in serum levels of alanine aminotransferase (ALT), aspartate aminotransferase, and gamma-glutamyl transferase, indicative of hepatocellular damage (fig. S1B). At age 20, she developed low serum albumin of 3.1 g/dl (normal values, 3.4 to 4.65 g/dl). A liver biopsy showed periportal lymphocytic infiltration and intense immunostaining for cytokeratin 7, indicative of bile duct proliferation which is known to be associated with chronic liver disease (Fig. 1F). Cytomegalovirus (CMV) and Epstein-Barr virus were not detected in the patient's blood. After a liver transplant for severe liver failure at age 22 years, she developed massive and persistent CMV viremia resistant to ganciclovir, valganciclovir, and letermovir. She died 11 months after transplant.

A homozygous $IKK\alpha^{Y580C}$ mutation was identified in the patient

A targeted next-generation sequencing panel for 264 genes associated with primary immunodeficiencies revealed no candidate variants. Whole exome sequencing (WES) identified a point mutation in *CHUK* (c.A1739G:p.Y580C) which encodes IKKα. The mutation is not present in the 1000 Genomes, ExAC, or NHLBI Exome Sequencing Project databases. This mutation is predicted to be pathogenic by Combined Annotation Dependent Depletion (CADD) (deleterious with a score of 26.3), PolyPhen-2 (probably damaging with a score of 0.99), and MutationTaster (disease causing). No other candidate genes were identified including the seven homozygous variants detected with a CADD score higher than 10 (table S1). Sanger sequencing revealed that the $IKK\alpha^{Y580C}$ mutation is homozygous in the patient and heterozygous in the parents and healthy siblings (Fig. 2, A and B). The Y580 residue is located within the helix-loop-helix (HLH) domain of IKKα (Fig. 2C) and is highly conserved among species (fig. S3). Structural modeling predicts that the Y580C mutation may disrupt a hydrogen bond between residues Y580 and D582 and cause local instability (Fig. 2D). The Y580C mutation did not affect IKKα protein expression in the patient fibroblasts (Fig. 2E).

The kinase function of IKKα is critical for activation of the noncanonical NF-κB pathway. An in vitro kinase assay, using purified recombinant wild-type (WT) or mutant $IKK\alpha^{Y580C}$ and $I\kappa B\alpha_{21–41}$ peptide as substrate, revealed that the intrinsic kinase activity of the mutant was intact (Fig. 2F). In contrast, activation of the noncanonical NF-κB pathway, which depends on ligand-induced NIK-mediated activation of IKKα, was severely impaired in the patient skin-derived fibroblasts, as evidenced by lack of p100 processing after cross-linking

of LTβR with agonistic anti-LTβR monoclonal antibody (mAb) (Fig. 2G). LTβR activation of the noncanonical NF-κB pathway up-regulates *VCAM1* expression in fibroblasts (8). The patient's fibroblasts failed to up-regulate *VCAM1* after LTβR ligation (Fig. 2H) but demonstrated intact *VCAM1* up-regulation after TNF-α stimulation, which activates the canonical NF-κB pathway (Fig. 2H).

The selective failure to activate the noncanonical NF-κB pathway in the patient's cells despite intact intrinsic kinase activity of the IKKα mutant prompted us to examine the interaction of NIK with the IKKα mutant. Human embryonic kidney (HEK) 293T cells were cotransfected with HA-tagged WT or mutant IKKα and Myc-tagged NIK followed by immunoprecipitation with anti-HA. Myc-NIK coimmunoprecipitated with HA-tagged WT IKKα but not HA-tagged mutant IKKα (Fig. 2I). Together, these data demonstrate that the Y580C IKKα mutation disrupts NIK binding and thereby selectively impairs noncanonical NF-κB signaling.

IKKα has a kinase-independent scaffolding function essential for driving the differentiation of epidermal keratinocytes (28). Thus, $IKK\alpha^{-/-}$ mice die shortly after birth due to massive transepidermal water loss (TEWL) but can be rescued by transgenic expression in keratinocytes of a kinase dead IKKα mutant, $IKK\alpha^{AA}$, in which the two serines whose phosphorylation is required for IKKα activation are replaced with alanine (24), indicating a critical role for IKKα scaffolding function in epidermal integrity. This scaffolding function involves the interaction in the nucleus of IKKα with the transcription factors SMAD2 and SMAD3 that are activated by TGFβ, resulting in the inhibition of TGFβ-driven proliferation of keratinocytes (29). Nuclear localization of the mutant IKKα and its interaction with SMAD2 and SMAD3 were comparable with WT IKKα (Fig. 2, J and K), consistent with a normal TEWL of 11.1 g/m^2 per hour in the patient. Thus, the Y580C mutation has no detectable effect on the kinase-independent scaffolding function of IKKα important for keratinocyte differentiation.

$IKK\alpha^{Y580C/Y580C}$ mice lack SLO

To further dissect the mechanism of the patient's disease, we ascertained that the binding of the mouse IKKα Y580C mutant to mouse NIK was impaired (fig. S4A) and then engineered homozygous $IKK\alpha^{Y580C/Y580C}$ mice using CRISPR-CAS9 gene editing. Murine embryonic fibroblasts (MEFs) from the mutant mice recapitulated the findings in the patient fibroblasts. They demonstrated normal expression of IKKα but impaired p100 phosphorylation and processing into p52 and defective induction of *Vcam1* after LTβR- but not TNF-α–driven activation (fig. S4, B to D). Furthermore, TNF-α–driven degradation of IκBα and phosphorylation of p65 were comparable in mutant and control MEFs (fig. S4E). Thus, $IKK\alpha^{Y580C/Y580C}$ mice, like the patient, exhibit a selective defect in noncanonical NF-κB activation.

$IKK\alpha^{Y580C/Y580C}$ mutant mice were born at the expected Mendelian ratio and appear normal at birth but die prematurely between 20 and 40 weeks of age (Fig. 3A). They also demonstrate poor weight gain; by 26 weeks of age, they weighed significantly less than WT controls (Fig. 3B). Mutant mice demonstrated defective bone fusion in the ribs (Fig. 3C). Most mutants (60%) developed conjunctivitis at about 20 weeks of age,

and some developed skin lesions (Fig. 3D) from which *Staphylococcus saprophyticus* could be cultured. Nonlesional skin of mutant mice had focal epidermal thickening and hyperkeratosis, was devoid of a significant dermal lymphoid infiltrate, and demonstrated significantly increased cell cycle activity within the basal cell layer, as evidenced by Ki-67 staining (Fig. 3E).

Gross examination of mutant mice revealed an absence of inguinal or mesenteric LNs or Peyer's patches (Fig. 3, F and G). Spleens of mutant mice had a normal cellularity (Fig. 3H) but severely disrupted architecture and a lack of defined follicles (Fig. 3I). Immunofluorescent staining for $MOMA^+$ macrophages revealed a disorganized marginal zone (MZ) structure (Fig. 3I). Splenic architecture was further investigated by staining for $Madcam1^+$ endothelial cells and $FDCM2^+$ follicular dendritic cells (FDCs). Both were markedly reduced in the mutant's spleen (Fig. 3I). Levels of IKKα comparable with WT controls were detected in mutant spleens (Fig. 3J). Mutant spleens had reduced expression of *Cxcl12* and *Cxcl13* (Fig. 3K), which depends on the noncanonical NF-κB pathway (30, 31).

$IKK\alpha^{Y580C/Y580C}$ mice have absent MZ B cells, reduced mature B cells, and fail to form germinal centers

B cell development in the bone marrow (BM) was normal in $IKK\alpha^{Y580C/Y580C}$ mice (Fig. 4A), consistent with it being largely independent of noncanonical NF-κB signaling (32). In contrast, BAFF signaling via the noncanonical NF-κB pathway is essential for peripheral B cell maturation and survival (33, 34). The proportions of recirculating mature B cells were reduced in the mutants' BM (Fig. 4A), and the mutants had diminished splenic B cell numbers (Fig. 4B). They also demonstrated a partial, yet significant, block between the transitional 1 (T1) and T2 stages of development (Fig. 4C and fig. S5A). Consistent with the absence of a MZ, mutant mice lacked MZ B cells (Fig. 4, C and D). The survival of mutant splenic B cells in the presence of BAFF was markedly impaired, despite normal levels of BAFF-R expression (Fig. 4E and fig. S5B). Unlike conventional B cells, which include peritoneal B-2 cells, peritoneal B-1 cells do not depend on noncanonical NF-κB signaling for their development and survival (35). $B220^{hi}IgM^+$ B-2 cells were markedly diminished in the peritoneum of mutant mice compared with WT controls (Fig. 4F). $B220^{int}IgM^+$ B-1 cells were increased ~2-fold in the mutant but secreted about half the amount of IgM compared with WT controls (Fig. 4F and fig. S5C).

Splenic B cells of $IKK\alpha^{Y580C/Y580C}$ mice had severely reduced proliferation in response to stimulation with mCD40L + IL-4 or lipopolysaccharide (LPS) + IL-4 (Fig. 4G), and significantly fewer viable cells were recovered at the end of the culture in comparison with WT controls (Fig. 4H). These findings were not associated with increased apoptosis or decreased cell viability (fig. S5, D and E). Further, activated mutant B cells failed to differentiate into $B220^{lo}CD138^+$ plasmablasts (Fig. 4I) and did not secrete IgM after LPS stimulation or immunoglobulin G (IgG) after mCD40L + IL-4 or LPS + IL-4 activation (Fig. 4J). These results indicate that the homozygous $IKK\alpha^{Y580C}$ mutation impairs B cell differentiation in vitro.

$IKK\alpha^{Y580C/Y580C}$ mice had a severe reduction in serum IgG and IgA levels but normal serum IgM levels (Fig. 4K). Mutant mice had an absent anti-trinitrophenol (TNP) antibody

response to intraperitoneal immunization with the T-independent (TI) antigen TNP-LPS and the T-dependent (TD) antigen TNP–keyhole limpet hemocyanin (KLH) (Fig. 4L). After intraperitoneal immunization with TNP-KLH, spleens from the mutant mice had significantly reduced numbers of $CD4^+CXCR5^+PD1^+$ T follicular helper (T_{FH}) cells compared with WT controls, and they virtually lacked $B220^+CXCR5^+GL7^+$ germinal center (GC) B cells (Fig. 4M). Moreover, GCs, detected by immunofluorescence staining of spleens for IgD, CD3, and GL7, were absent from mutant mice intraperitoneally immunized with TNP-KLH (Fig. 4N). It has been shown that circulating T_{FH} cells develop independently of B cells (36). The percentage of circulating T cells among $CD4^+$ FH cells 8 days after TNP-KLH immunization was comparable in the mutants and WT controls (fig. S5F), suggesting that the reduction in splenic T_{FH} cells in the mutant is primarily due to the virtual lack of B cells. These findings indicate that the homozygous $IKK\alpha^{Y580C}$ mutation severely impairs B cell function.

T cells from $IKK\alpha^{Y580C/Y580C}$ mice have impaired IL-2 and IL-17A production in vitro and fail to respond to cutaneous immunization with antigen

The numbers of splenic $CD3^+$ T cells and the percentages $CD3^+CD4^+$ and $CD3^+CD8^+$ subsets were comparable in $IKK\alpha^{Y580C/Y580C}$ mice and WT controls (Fig. 5A). However, the percentage of $CD4^+FOXP3^+$ regulatory T cells (T_{regs}) among splenic $CD4^+$ T cells was significantly reduced in the mutant (Fig. 5B). Within their $CD4^+$ T cell compartment, mutant mice demonstrated a significant reduction of $CD62L^{lo}CD44^{hi}$ T effector/effector memory (T_{EM}) cells and $CD62L^{hi}CD44^{hi}$ T central memory (T_{CM}) cells but an increase in $CD62L^{hi}CD44^{lo}$ naïve T cells (Fig. 5C). In vitro mitogenic T cell stimulation with $\alpha CD3^+$ $\alpha CD28$ antibodies resulted in proliferation and cellularity comparable between mutant mice and WT controls (Fig. 5, D and E). IL-2 and IL-17A secretion by T cells was, however, significantly reduced in mutant mice, whereas secretion of IFN-γ, IL-4, and IL-13 was similar to WT controls (Fig. 5F and fig. S6).

After intraperitoneal immunization, the interaction of antigenic-specific T cells with peptide major histocompatibility complex (MHC) class II complexes on the surface of antigen-presenting cells occurs in the spleen and mesenteric LNs, whereas after following epicutaneous (EC) immunization, it occurs in skin-draining LNs. The T cell response to immunization with the antigen ovalbumin (OVA) was assessed by examining cytokine secretion by splenocytes in response to restimulation with OVA ex vivo. After intraperitoneal immunization, the mutants demonstrated modestly decreased IL-2 secretion, severely reduced IL-17A secretion, but normal IFN-γ secretion compared with WT controls (Fig. 5G). After EC immunization by repeated application of OVA to tape-stripped skin over 12 days (Fig. 5H), splenocytes from WT mice secreted robust amounts of IL-2, IL-17A, and IFN-γ, but secretion of all three cytokines was abolished in splenocytes from EC-immunized mutants (Fig. 5H), consistent with the lack of LNs.

Reduced cutaneous *Il17a* expression and susceptibility to *S. aureus* skin infection in $IKK\alpha^{Y580C/Y580C}$ mice

The patient suffered from recurrent skin infections with *S. aureus* and *Candida albicans*. IL-17A plays an important role in containing these infections in part by driving

keratinocytes to produce anti-microbial peptides (AMPs) (37). TCR$\gamma\delta^+$ cells are the main source of IL-17A in the skin at baseline and after intradermal exposure to *S. aureus* (38). Expression of *Il17a* was undetectable in the mutants' skin (Fig. 6A), although it had normal numbers of TCR$\gamma\delta^+$ cells (Fig. 6B). The mutants demonstrated impaired cutaneous clearance of PSVue 794–labeled *S. aureus* Methicillin-resistant *Staphylococcus aureus* (MRSA) strain SF8300 (USA300) as measured by whole animal bioluminescence and numbers of colony-forming units (CFU) in skin homogenates (Fig. 6, C and D). IL-17A expression by TCR$\gamma\delta^+$ cells in *S. aureus* infected skin is up-regulated in response to IL-1 and IL-23. Expression of *Il17a*, but not *Il1b* nor *Il23a* (p19), was markedly reduced in *S. aureus* infected skin of the mutants compared with WT controls (Fig. 6, E and F). Furthermore, expression of the IL-17A regulated AMP genes *Reg3b*, *Def14b*, and *Camp* was significantly lower in the mutants' infected skin (Fig. 6G).

IKKα interacts with and phosphorylates RAR-related or- phan receptor gamma T (RORγt). Binding of the IKKα-RORγt complex to the *Il17a* promoter results in IKKα-dependent phosphorylation of Histone 3 and enhanced *Il17a* expression (39). The IKKα domain involved in binding to RORγt is not known. The ability of the IKKα^{Y580C} mutant to bind to RORγt was examined in 293T cells cotransfected with hemagglutinin (HA)–tagged mutant or WT IKKα and Myc-tagged RORγt. Comparable amounts of hemagglutinin (HA)-tagged mutant and WT IKKα were detected in Myc immunoprecipitates (Fig. 6H). Thus, the Y580C mutation preserves IKKα binding to RORγt. As NIK-deficient mice have impaired *Il17a* expression (40), defective interaction of the IKKα^{Y580C} mutant with NIK likely underlies the defective *Il17a* expression in the mutant mice.

Developmental and functional defects in the thymus of IKKα$^{Y580C/Y580C}$ mice enable expansion of potentially autoreactive T cell clones

Thymi of 4- to 6-week-old mutant mice had a normal cellularity and normal frequencies of CD4$^-$CD8$^-$ double-negative (DN), CD4$^+$CD8$^+$ double-positive (DP), and CD4$^-$CD8$^+$ single-positive (CD8SP) thymocytes but demonstrated a significant increase in the percentage of CD4$^+$CD8$^-$ single-positive (CD4SP) cells (Fig. 7, A and B, and fig. S7A). Both absolute thymic cellularity and percentage of CD4^{+-} FOXP3$^+$ natural T_{regs} within the CD4SP compartment were significantly decreased (Fig. 7C and fig. S7B).

Noncanonical NF-κB signaling is essential for the development of medullary (m) TECs, which present autoimmune regulator (AIRE)- and FEZ family zinc finger 2 (FEFZ2)–regulated tissue-restricted antigens to SP thymocytes, thereby purging self-reactive clones and establishing central T cell tolerance (41–43). Histological analysis of the thymus revealed an effaced corticomedullary junction and severely decreased staining for AIRE and Ulex europaeus agglutinin-1 (UEA-1) expressed by mTECs (Fig. 7D and fig. S5C). Flow cytometry analysis revealed markedly reduced total TECs (CD45$^-$EPCAM-1$^+$) cellularity in mutant mice compared with WT controls (Fig. 7E). This reduction affected both cortical (c) TECs (Ly51$^+$ UEA1$^-$) and mTEC (Ly51$^-$ UEA1$^+$) but was primarily due to a virtual lack of the latter population (Fig. 7E and fig. S7D).

LTβR signaling is important in the development of medullary thymic fibroblasts (mFb), which are important for mTEC development and thus for central tolerance (44).

The number of thymic $CD45^{-}Ter119^{-}EpCAM1^{-}CD31^{-}gp38^{+}CD26^{-}$ mFb, but not of $CD45^{-}Ter119^{-}EpCAM1^{-}CD31^{-}gp38^{+}CD26^{+}$ thymic capsular fibroblasts (capFb), was significantly reduced in mutant mice compared with WT controls (fig. S7E). Transcriptome analysis revealed that the mutant mFbs had a diminished expression of 25 of the 100 top mFb-specific genes, whereas gene expression in capFb was largely unaffected (fig. S7F).

Two major waves of thymocyte negative selection shape the T cell receptor (TCR) repertoire and take place sequentially first in the cortex (wave 1) and then in the medulla (wave 2) (45). The combined expression of the transcription factor HELIOS and the cell surface marker programmed cell death protein 1 (PD1) identifies thymocytes that have been subject to wave 1 negative selection, whereas the expression of HELIOS among medulla-resident ($CCR7^{+}$) thymocytes identifies cells that have undergone wave 2 negative selection (45). The percentage of $CD4^{+}CD8^{+}TCR\beta^{hi}CD44^{-}CCR7^{-}FOXP3^{-}PD1^{+}HELIOS^{+}$ DP cells undergoing the first step of the cortical selection (wave 1a) was minimally increased in mutant mice (Fig. 7F, left two) whereas the frequency of $CD4^{+}CD8^{-}TCR\beta^{hi}$ $CD69^{+}CD44^{-}CCR7^{-}FOXP3^{-}CD25^{-}HELIOS^{+}PD1^{+}$ immature CD4SP thymocytes undergoing the second step of the cortical selection (wave 1b) was comparable for mutant and control mice (fig. S7G). In contrast, both steps of thymocyte negative selection in the medulla were compromised in mutant mice as the frequencies of $CD4^{+}CD8^{-}TCR\beta^{hi}CD69^{+}CD44^{-}CCR7^{+}FOXP3^{-}CD25^{-}HELIOS^{+}$ semimature CD4SP cells (wave 2a) and of $CD4^{+}CD8^{-}TCR\beta^{hi}$ $CD69^{-}CD44^{-}CCR7^{+}FOXP3^{-}CD25^{-}HELIOS^{+}$ mature CD4SP cells (wave 2b) were severely reduced when compared with WT controls (Fig. 7F, middle and right two). Consistent with these results, the percentage of thymocytes that have just advanced past positive selection in the cortex (as identified by a $TCR\beta^{hi}CD69^{hi}$ phenotype) was comparable for mutant mice and WT controls. However, the frequency of thymocytes at later maturational stages (as marked by a $TCR\beta^{hi}CD69^{-}$ phenotype and typically resident in the medulla) was higher in the mutant compared with WT controls (fig. S7H) (46). The frequencies of unselected $TCR\beta^{low}CD69^{-}$ and $TCR\beta^{int}CD69^{int}$ thymocytes were unaffected in mutants (fig. S7H).

We next analyzed at the population level the TCRVβ CDR3 regions of mature $CD25^{-}CD44^{lo}$ CD4SP thymocytes (designated CD4SP M2 thymocytes) excluding T_{regs} and recirculating CD4SP cells from the analysis (47, 48). The mutants had significantly fewer unique CDR3s resulting in a reduced TCRVβ repertoire diversity and diminished Shannon entropy (Fig. 7G). The potential auto-reactivity of a specific CDR3 sequence can be predicted by the hydrophobicity index of the amino acid residues at position 6 and 7 of CDR3 (49). CDR3 sequences from sorted M2 cells demonstrated a significantly higher hydrophobicity index in the mutants compared with WT controls (Fig. 7H). The results of this computational analysis suggest that a greater proportion of CDR3 sequences are reactive in the mutants to tissue-restricted antigens (TRA) (also known as self). Together, these findings demonstrate that the homozygous Y580C mutation in IKKα disrupts mTEC-driven negative selection of CD4SP thymocytes leading to the expansion of cells with a potentially autoreactive TCR specificity.

Organs of IKKα$^{Y580C/Y580C}$ mice are infiltrated by activated T cells and show evidence of tissue damage

The escape of potentially autoreactive T cell clones from thymocyte negative selection led us to probe the periphery of mutant mice for evidence of autoimmune inflammation. Histologic examination of mice organs at 26 weeks of age revealed mixed lymphocytic and neutrophilic infiltrates in pancreas periductal and islets adjacent areas, lung perivascular areas, and liver periportal areas in mutant mice, but not WT littermate controls (Fig. 8A and fig. S8, A and B). Sera from mutant mice showed no IgG reactivity against mouse stomach tissue sections (fig. S8C). IHC staining demonstrated that the majority of lymphocytes infiltrating the organs of the mutants were CD3$^+$ T cells (Fig. 8A). The numbers of CD4$^+$ and CD8$^+$ T cells recovered from liver, pancreas, and lung were significantly higher in mutant mice compared with WT controls (Fig. 8B and fig. S9, A and B). Flow cytometric analysis revealed that the percentages of CD4$^+$ and CD8$^+$ T cells expressing CD25 and CD69 in these organs, as well as the level of CD25 and CD69 expression by these infiltrating T cells, were significantly higher in the mutants compared with WT controls (Fig. 8, C and D, and fig. S9, C and D). Moreover, the percentages of CD62L^{lo}CD44^{hi} CD4$^+$ and CD8$^+$ effector/effector memory T cells and the level of CD44 expression by these cells were significantly higher in the mutants compared with WT controls (Fig. 8E). In contrast, neither the percentages of splenic CD4$^+$ and CD8$^+$ T cells that were CD25$^+$, CD69$^+$, or CD62L^{lo}CD44^{hi} cells nor the levels of CD25, CD69, or CD44 expression by these cells were increased in the mutants compared with WT controls (fig. S9, E and F). We did not observe T cell infiltrates in the mutants' skin or colon (fig. S9, G and H).

Immunofluorescence examination of the liver revealed cellular damage as evidenced by increased expression of activated caspase-3 and receptor-interacting protein kinase 3 (RIP3) (Fig. 8F). Increased ALT levels and decreased albumin levels were observed in the serum of mutant mice, indicative of hepatocellular damage and impaired liver function (Fig. 8G). There was also decreased insulin and amylase levels in the serum revealing impaired pancreatic endocrine and exocrine functions, respectively (Fig. 8H). Moreover, serum lactate dehydrogenase (LDH) levels were significantly elevated in mutant mice (Fig. 8I), indicative of increased cell turnover. Together, these data indicate that the homozygous IKKα^{Y580C} mutation results in a breakdown of T cell tolerance resulting in autoimmune organ inflammation and injury.

DISCUSSION

We identified IKKα deficiency caused by a homozygous p.Y580C mutation in IKKα as a previously undescribed cause of combined immunodeficiency and recapitulated the patient's complex findings in a mouse model of the disease. The Y580 residue in IKKα mutated in the patient is located in the HLH domain, a region important for IKKα interaction with NIK (14). In particular, an IKKα double mutant in which Y580 and the adjacent residue H578 are mutated to alanine lacks the capacity to bind NIK (14). The IKKα^{Y580C} mutant protein is expressed normally and retains intrinsic kinase activity but fails to bind NIK. Intact intrinsic kinase activity of the IKKα^{Y580C} mutant is not unexpected as the mutated Y580 residue is located in a solvent exposed region distinct from the kinase domain as

determined by crystallography. Fibroblasts from the patient and mutant mice fail to process NF-κB2/p100 into p52 and can therefore not activate the noncanonical NF-κB pathway after LTβR ligation. Furthermore, the patient shares several features with patients with defects in NIK, NF-κB2/p100, and RelB components of the noncanonical NF-κB pathway (19–21). These include susceptibility to bacterial, viral, and fungal infections and failure to develop SLO, B cell lymphopenia, hypogammaglobulinemia, and autoimmunity (19–21).

The patient demonstrated an incomplete fusion of sternal and sacral bones, and mutant mice showed defective fusions of rib bones. NIK-dependent IKKα-mediated RANKL-RANK signaling in chondrocytes is important for cartilage to bone maturation (50). Defective RANKL-RANK signaling may therefore account for the skeletal abnormalities observed in the patient and mutant mice. Keratinocyte differentiation in the patient and mutant mice and the interaction of $IKK\alpha^{Y580C}$ with SMAD2/3 proteins, which is important for keratinocyte differentiation, were both normal. The development of spontaneous dermatitis in IKKα mutant mice, as in NIK-deficient mice (51), suggests that NIK activation of IKKα protects from the development of dermatitis, possibly by contributing to the up-regulation of epidermal genes that are important for the repair of the skin barrier (52–55).

Formation of SLO is dependent on LTβR-driven noncanonical NF-κB signaling in mesenchymal lymphoid tissue organizer stromal cells after engagement of their LTβR by membrane bound LTα1β2, expressed by hematopoietic lymphoid tissue inducer (LTi) cells, or by endothelial cells after RANKL-RANK–mediated interaction with LTi cells (56, 57). Consistent with disrupted noncanonical NF-κB signaling, the patient had no palpable LNs or a Waldeyer’s ring, and mutant mice lacked LNs and Peyer’s patches. In addition, mutant mice demonstrated a disrupted architecture of the spleen with a lack of follicles, the absence of MZs, paucity of $MOMA^+$ macrophages, and a marked reduction in FDCs. The lack of SLO is likely due to mutant stromal cells deficient expression of chemokines (as demonstrated for *Cxcl12* and *Cxcl13* in mice) and adhesion molecules (e.g., *VCAM1* as shown in the patient and mice) necessary for lymphorganogenesis.

T cell numbers were normal in the patient’s blood at presentation and in the spleens of mutant mice. In addition, $CD4^+$ memory T cells were reduced in the spleen of the mutants. These observations are consistent with previous findings that disruption of noncanonical NF-κB signaling has little effect on total T cell cellularity but impairs the generation of T effector cells (21, 58, 59). Unlike mutant mice, the patient did not have a reduction in $CD4^+$ memory T cells. This could be due to intense microbial exposure in the patient compared with the specific pathogen–free (SPF) conditions in which the mice were reared. T cell proliferation to polyclonal stimulation was normal both in the patient and mutant mice. T cells from the mutants had normal IFN-γ secretion but diminished IL-2 secretion and markedly reduced IL-17A secretion after ligation of CD3 and CD28. The preserved antigen-driven T cell secretion of IFN-γ after intraperitoneal immunization in mutant mice suggests that, in the absence of LNs, education and expansion of antigen-specific T cells can occur in the spleen despite a disorganized splenic architecture. This supposition is consistent with the relative evolutionary independence of a T cell response from the formation of secondary lymphoid structures (60). IKKα functionally associates with Vav to induce NF-κB activation in response to CD28 engagement (61); this possibly underlies the defective

IL-2 secretion. The IKKα mutant interacted normally with RORγt, which recruits IKKα to the *Il17a* promoter where it phosphorylates Histone 3. Failure of the mutant to be activated by NIK may explain the impaired *Il17a* expression, a feature shared with NIK deficiency. Impaired *Il17a* expression likely underlies the susceptibility of the mutant to cutaneous *S. aureus* infection. No detectable antigen-specific responses were elicited in the mutants after EC sensitization with OVA, illustrating the critical importance of draining LNs as a platform where recirculating antigen-specific naïve T cells encounter tissue-derived antigen-laden DC emigrants.

The IKKα mutation had a marked effect on peripheral B cell number and function. The patient presented in infancy with severe panhypogammaglobulinemia and B cell lymphopenia that markedly worsened with age. B cell development in the BM was unaffected in mutant mice, but peripheral maturation, which depends on BAFF-R signaling via the noncanonical NF-κB pathway, was impaired. Consistent with the absence of a MZ, mutant mice demonstrated an absence of MZ B cells and failed to mount an antibody response to the TI antigen TNP-LPS. They also failed to mount an antibody response to intraperitoneal immunization with the TD antigen TNP-KLH, despite the generation of T_{FH} cells, albeit in reduced numbers. This was associated with the failure to form GCs and the virtual absence of GC B cells. Similar findings have also been observed in other mutant mice with disrupted lymphorganogenesis (62–69) illustrating the stringent dependence of B cell responses to TD antigens on well-organized secondary lymphoid structures (70).

The thymus of mutant mice demonstrated an effacement of the corticomedullary junction, a virtual lack of mTECs, and decreased numbers and altered gene signature of mFbs, which are important for the development of mTECs. LTβR signaling is essential for the development of mTECs, mFbs, and organization of the thymic medulla (71). LTβR, CD40, and RANK signaling in mTECs drive the expression of the transcription factor AIRE, whereas LTβR signaling enables a normal expression of the transcription factor FezF2 (72, 73). AIRE and FezF2, in turn, control the expression of complementary sets of TRA that orchestrates the deletion of T cells with high affinity TCR directed against antigens, thus enforcing a deletional form of central T cell tolerance. In parallel, promiscuous gene expression in the thymic medulla promotes the development of natural T_{regs}, which enforce peripheral tolerance (74, 75). The lack of mTECs in mutant mice led to defective negative selection in the medulla, a restricted TCRVβ repertoire at the population level and an expansion of potentially autoreactive T cell clones. Recently, T cell self-reactivity and autoimmune susceptibility have been reported in the presence of NF-κB2/p100 variants (76). Consistent with a role of mTECs in their generation, T_{regs} were decreased in the thymus and spleen of the IKKα mutants, a feature shared with animals deficient in NIK, NF-κB2/p100, and RelB (77–81).

The patient’s liver and intestines were infiltrated by T cells. Similarly, the mutant mice demonstrated infiltration of the liver, pancreas, and lungs by activated T cells, as well as organ damage, which likely contributed to the early mortality of these mice. Failure of both central and peripheral tolerance may have contributed to T cell autoimmunity. In contrast to our mutant mice, mice homozygous for an IKKα kinase dead mutant do not exhibit organ infiltration by T cells, although they lack mTECs and have decreased number of T_{regs}

(82). Thus, our studies provide unique structure-function insights into the role of IKKα in immunity and self-tolerance.

Unlike the patient exposed to natural flora, mutant mice raised under SPF conditions lacked T cell infiltrates in the skin and colon, two tissues normally heavily exposed to microbes. This suggests that the microbiome may be an important driver of T cell infiltration into mucosal sites in the patient. Defective IL-17A production, as well as defective intestinal M cell function, which depends on noncanonical NF-κB signaling (83), may have contributed to the susceptibility of the patient to a highly diverse intestinal microbiome and infections.

In summary, this study identifies IKKα deficiency as a newly identified cause of combined immunodeficiency associated with autoimmunity and demonstrates that the IKKα Y580 residue is critical for NIK binding and thereby for the activation of the noncanonical NF-κB pathway.

MATERIALS AND METHODS

Human studies

Skin biopsies for establishing fibroblast lines in patient and controls were performed after securing informed consent. Tissue biopsies from archived samples from patients and healthy controls (HCs) were used.

Human tissue histology

Biopsy sections prepared from samples fixed in 10% buffered formalin and paraffin embedded were stained with hematoxylin and eosin (H&E). Immunohistochemistry (IHC) was performed using rabbit anti-Ki67 mAb (TM Ventana), rabbit anti-HPV mAb (clone K1H8, Dako, Carpinteria, CA), mouse anti-CD3 mAb (1:100; LN10, Novocastra), and mouse anti-Human Cytokeratin 7 (clone OV-TL 12/30 Dako/Agilent).

WES and Sanger sequencing

WES and Sanger sequencing were performed as previously described (84). In brief, 10 μg of genomic DNA were isolated from peripheral blood samples using the Gentra Puregene blood kit (QIAGEN), as per kit protocol. Next-generation sequencing was performed using the Primary Immunodeficiency Disease (PID) v2 panel and Ion Torrent S5 sequencer (Thermo Fisher Scientific). Coverage analysis and variant calling were performed using Ion Reporter software (Thermo Fisher Scientific). WES of patient was performed with an Illumina HiSeq-2000. The paired-end Illumina libraries were captured in solution according to the Agilent Technologies SureSelect protocol with 101–base pair (bp) read length. The sequence data were mapped to the human reference genome (hg-19, NCBI37) using the Burrows-Wheeler alignment method at default settings. Variants were identified with the Genome Analysis Toolkit, SAMTools, and Picard Tools (http://broadinstitute.github.io/picard/). Variants with a read coverage of <2 times or Phred-scaled, single-nucleotide polymorphism quality of <20 were discarded.

Sanger sequencing was used to validate the missense mutation in *CHUK* identified by WES in the affected patient, sibling, and control. Amplification and sequencing

primers were made to amplify the nucleotide sequence surrounding the mutated base pairs in *CHUK* (Fp1: 5′-GAGAATGAGTGAGCCTTGTTTAAT-3′, Rp: 5′-AACCTCTGTGATTTAATAGGAGAC-3′, SFp: 5′-GGCAGCGAATCTTTTATGTAAC-3′, SRp: 5′-CAAAACCAAAACAAAATGTGCG-3′).

Protein model

The IKKα^{Y580C} mutant protein was modeled using PyMOL and the crystal structure of human IKK1 available in the Protein Data Bank (PDB ID 5EBZ).

Immunoblotting

Cells were lysed in phosphate-buffered saline (PBS) that contains 30 mM tris-HCl (pH 7.5), 120 mM NaCl, 2 mM KCl, 1% Triton X-100, and 2 mM EDTA supplemented with a protease inhibitor (Roche). Proteins were separated by electrophoresis on 4 to 15% precast polyacrylamide gels (Bio-Rad) and were transferred to 0.45 μm of nitrocellulose membrane (Bio-Rad). Membranes were blocked in a 1× solution tris-buffered saline/Tween 20 (TBS-T) with 5% nonfat dry milk for 1 hour at room temperature and then incubated overnight at 4°C with the specified primary antibody. Antigen-antibody complexes were visualized with peroxidase-conjugated secondary antibodies (GE Healthcare) and enhanced chemiluminescence Western blotting substrate (Pierce). Densitometry of immunoblots was done using the ImageJ analyzer software (1.48v).

Primary antibodies used in immunoblots were as follows: rabbit mAbs to β-actin (Cell Signaling Technology, 4970), HA tag (Cell Signaling Technology, 3724), IKKα (Cell Signaling Technology, 2682), NF-κB2 (p100/p52), (Cell Signaling Technology, 4882), NIK (Cell Signaling Technology, 4994), α-tubulin (Cell Signaling Technology, 2144), Lamin A/C (Cell Signaling Technology, 2032), SMAD2/3 (Cell Signaling Technology, 8685), and mouse mAb to Myc (Cell Signaling Technology, 2276). All secondary antibodies were obtained from the Jackson ImmunoResearch Laboratory.

Transfection of HEK293T cells

HEK293T cells were seeded in six-well plates at a density of 2.5×10^5 cells per well and in Dulbecco's modified Eagle's medium (DMEM) with 10% fetal calf serum. WT and mutant IKKα encoding plasmids (0.2 μg of DNA) were combined with 7.5 μl of TransIT-LT1 Transfection Reagent (Mirus Bio LLC, Madison, WI) in DMEM and incubated at room temperature for 30 min. The mixture was added dropwise to seeded cells, and the cells were incubated for 24 hours.

Coimmunoprecipitation of IKKα with NIK and RORγt

HEK293T cells transfected with HA-tagged WT or mutant IKKα encoding plasmids and with plasmids encoding Myc-tagged NIK or Myc-tagged RORγt were lysed in cell lysis buffer (Cell Signaling Technology product no. 9803) supplemented with protease inhibitors. Lysates were incubated with Protein G Sepharose beads (GE Healthcare, 17-0618-01) and anti-HA Ab or IgG Rabbit isotype overnight at 4°C. Beads were washed with TBS-T, diluted in sample buffer with BME (2-mercaptoethanol), and boiled for 5 min.

Coimmunoprecipitation of IKKα and SMAD2/3

Lysates of HEK293T cells transfected with HA-tagged WT or mutant IKKα encoding plasmids prepared as above were incubated with human recombinant SMAD2/3 and anti-HA Magnetic Agarose beads (Pierce, #88836) overnight. The magnetic beads were collected with a magnetic stand and washed with TBS-T. Bound protein was eluted with 100 μl of 50 mM NaOH on a rotator for 5 min at room temperature. The beads were magnetically removed from the sample, and the sample was neutralized by adding 50 μl of 1 M tris (pH 8.5).

Nuclear extraction

Nuclear extracts were prepared from transfected HEK293T cells using a Nuclear Extract Kit (Active Motif 40010).

Kinase assay of IKKα enzymatic activity

HEK293T cells transfected with WT and mutant IKKα encoding plasmids were lysed in cell lysis buffer (Cell Signaling Technology product no. 9803) supplemented with protease inhibitors. Lysates were incubated with anti-HA Magnetic Agarose beads (Pierce, #88836) for 1 hour and eluted with competitive peptide (Thermo Fisher Scientific product no. 26184), and the relative concentrations of IKKα WT and mutant proteins were quantified by immunoblotting an equal volume aliquot from each. IKKα enzymatic activity was determined using ADP-Glo IKKα Kinase Enzyme System (Promega, V4068). WT and mutant IKKα were incubated with a peptide substrate derived from IκBα (amino acids 21 to 41) in kinase assay buffer [40 mM tris, 20 mM $MgCl_2$, bovine serum albumin (BSA; 0.1 mg/ml), and 50 μM dithiothreitol] for 120 min, and luminescence was measured using the Beckman Coulter DTX 880 Multimode Detector (Beckman Coulter, Brea, CA). Luminescence values were normalized to protein input based on the quantification of IKKα protein.

Gene expression analysis

mRNA was extracted from fibroblasts and total skin using an RNeasy Mini kit (QIAGEN) and was reverse-transcribed with the SuperScript VILO cDNA synthesis kit (Thermo Fisher Scientific). Gene expression was measured using quantitative polymerase chain reaction (PCR) in TaqMan Fast Advanced Master Mix (Applied Biosystems). Experiments were run on a QuantStudio 3 Real-Time PCR System (Applied Biosystems). The expression of genes was analyzed using the $2^{-\Delta\Delta CT}$ method in comparison with the housekeeping gene *Gapdh* (12). The following probes were used: *VCAM1* (Hs01003372), *Vcam1* (Mm01320970), *Cxcl12* (Mm00445553), *Cxcl13* (Mm00444533), *Il17a* (Mm00439618), *Il1b* (Mm00434228), *Il23a* (Mm00518984), *RegIIIb* (Mm00440616), *Def14b* (Mm00806979), and *Camp* (Mm00438285).

Generation of IKKa$^{Y580C/Y580C}$ mice

Single guide RNA (sgRNA) design was facilitated though the CRISPR Design tool (crispr.mit.edu) to minimize off-target effects. A guide was selected that was predicted to generate a double-stranded break 4 nucleotides from the intended c.1739 A>G p.Y580C

mutation. A 160-bp repair template was designed that included the c.1739 A>G mutation as well as synonymous c.1944C>T change in the protospacer adjacent motif to prevent repair template-targeting by the CAS9 nuclease. C57BL/6 zygotes were microinjected with CAS9 mRNA (System Biosciences), a single-stranded repair template oligo (PAGE Ultramer from Integrated DNA Technologies), and the sgRNA. For sgRNA synthesis, the T7 promoter sequence was added to sgRNA template/forward primer, and the in-vitro transcription (IVT) template was generated by PCR amplification. The T7-sgRNA PCR product was purified and used as the template for IVT using MEGAshortscript T7 kit (Life Technologies). The sgRNA was purified using the MEGAclear kit (Life Technologies). Aliquots from an IVT reaction were separated on agarose gel to assess reaction quality. Mutant mice were backcrossed on a C57BL/6 background for six generations.

Mouse tissue histology and immunofluorescence

Tissue was fixed in 4% paraformaldehyde, then embedded in paraffin, and were cut into 4-μm sections that were stained with H&E, Ki67, and CD3 or were processed for immunofluorescence staining. For Ki67, the epidermal layer in a minimum of three randomly selected histologic fields was examined at 400× magnification, and all nucleated epidermal cells were counted. In general, the epidermal width represented in one 400× field is 0.5 mm, so in total, at least 1.5 linear mm of randomly selected epidermal width was quantified. For immunofluorescence, slides were washed in PBS and blocked with 10% goat serum supplemented with 1% BSA/PBS for 1 hour and then incubated overnight with primary antibody in 2% BSA/PBS. Conjugated secondary antibodies were added to the slides and incubated for 1 hour. The slides were then mounted with ProLong Diamond Antifade Mountant (Thermo Fisher Scientific). To detect autoantibody to stomach antigen, serum was diluted 1:40 in 1× PBS fluorescein isothiocyanate and incubated on slides containing mouse stomach sections.

Cell stimulations

Skin fibroblast cell lines were derived from a skin biopsy from the patient and HCs. Fibroblasts were grown in DMEM supplemented with 10% fetal bovine serum, 50,000 IU of penicillin, 50,000 μg of streptomycin, 10 μM Hepes, and 2 mM glutamine. Patient and control fibroblasts were stimulated for 24 or 48 hours with either α-LTBR (10 μg/ml) (BioLegend, 31G4D8) or TNF-α (20 ng/ml) (InvivoGen).

Cellular proliferation of freshly isolated NK cells was evaluated by detecting intracellular Ki-67. PBMCs derived from patient and from healthy donor were stimulated with recombinant human IL-2 (100 U/ml) (Proleukin; Chiron) at 37°C for 48 hours. PBMCs were permeabilized with saponin solution (0.1% in PBS) at 4°C for 20 min. Then, cells were incubated with Ki-67 mAb as primary antibody (1:40 dilution; IgG1, mouse anti-human, Dako) for 1 hour at 4°C to detect the nuclear proliferation antigen. The secondary antibody used was phycoerythrin (PE)–conjugated isotype-specific goat anti-mouse (Southern Biotechnology) and was incubated for 30 min at 4°C, and then cells were resuspended in 500 μl of PBS solution for flow cytometry analysis.

To detect intracellular production of IFN-γ, PBMCs derived from patients and from healthy donors were incubated overnight at 37°C with IL-12 (20 ng/ml, PeproTech) plus IL-18 (100 ng/ml, PeproTech). Cells were then washed, fixed, and permeabilized with a BD Cytofix/Cytoperm kit (BD Biosciences Pharmingen). IFN-γ production was detected by subsequent intracellular staining with anti–IFN-γ–PE (BD Biosciences Pharmingen) upon gating on $CD56^+CD3^-CD14^-CD20^-$ cells. For IFN-γ expression experiments, the percentage of positive cells was calculated subtracting the baseline of IFN-γ expression in control cultures in the absence of stimuli (cytokines).

Splenic total B and T cells were isolated using the CD43 (Ly48) or Pan T cell microbeads kits (Miltenyi), respectively, and peritoneal B-1 B cells ($B220^+IgM^+CD5^+$) were sorted (Sony, MA9000) then cultured in RPMI supplemented with 10% fetal bovine serum, penicillin/streptomycin, 10 μM Hepes, 2 mM glutamine, and BME. B cells were stimulated at 37°C for 72 hours with LPS (10 μg/ml, InvivoGen), mCD40L (Enzo: 0.3 μg/ml) with mouse rIL-4 (50 ng/ml, Miltenyi) or with rBAFF (Enzo), and rIL-4 for 96 hours. T cells or splenocytes were seeded at 1×10^6 cells/ml in 5-ml culture tubes and were then stimulated at 37°C for 72 hours with $\alpha CD3^+$ αCD28 Dynabeads (bead-to-cell ratio of 1:1; Thermo Fisher Scientific) or with OVA (200 μg/ml), respectively. Supernatants and cells were collected and stored at −80°C for future analysis or stained for fluorescence-activated cell sorting (FACS).

Flow cytometry

Standard flow cytometric methods were used for the staining of cell-surface and intracellular proteins. Anti-mouse mAbs with the appropriate isotype-matched controls were used for staining. All flow cytometry data were collected with an LSR Fortessa (BD Biosciences) cell analyzer and analyzed with FlowJo software (Tree Star).

Reagents and mAbs for flow cytometry FACS were used as described by the manufacturer: annexin V (BioLegend, 640912), CellTrace Violet (CTV) (Thermo Fisher Scientific, C34557), and mAbs to CCR7 (BioLegend, 4B12), CD11b (BioLegend, M1/70), CD11c (Thermo Fisher Scientific, N418), CD138 (BioLegend, 281–2), CD185 (CXCR5) (BioLegend, L138D7), CD21/CD35 (Thermo Fisher Scientific, 8D9), CD23 (Thermo Fisher Scientific, B3B4), CD24 (BioLegend, M1/69), CD25 (BioLegend, PC61), CD26 (DPP-4) (BioLegend, H194–112), CD278 (ICOS) (BioLegend, 15F9), CD279 (PD1) (Thermo Fisher Scientific, J43), CD3 (Thermo Fisher Scientific, 145–2C11), CD31 (BioLegend, MEC13.3), CD4 (BioLegend, RM4–5), CD43 (Thermo Fisher Scientific, eBioR2/60), CD44 (Thermo Fisher Scientific, IM7), CD45 (BioLegend, 30-F11), CD45R (B220) (Thermo Fisher Scientific, RA3–6B2), CD49b (Thermo Fisher Scientific, DX5), CD5 (Thermo Fisher Scientific, 53–7.3), CD54 (ICAM-1) (Thermo Fisher Scientific, YN1/1.7.4), CD62L (BioLegend, MEL-14), CD69 (BioLegend, H1.2F3), CD8 (BioLegend, 53–6.7), CD93 (Thermo Fisher Scientific, AA4.1), CD95 (FAS) (Thermo Fisher Scientific, 15A7), Ep-CAM (BioLegend, G8.8), FDC-M2 (ImmunoK, FDC-M2), FOXP3 (Thermo Fisher Scientific, FJK-16 s), GL7 (Thermo Fisher Scientific, GL7), HELIOS (BioLegend, 22F6), IFN-γ (BioLegend, XMG1.2), IgD (Thermo Fisher Scientific, 11–26c), IgM (Thermo Fisher Scientific, II/41), Ki67 (BD Pharmingen, B56), Ly51 (BioLegend, 6C3), Ly6G

(BioLegend, 1A8), MHC Class II (I-A/I-E) (Thermo Fisher Scientific, M5/114.15.2), PD1 (BioLegend, RMP1–30), Podoplanin (gp38) (BioLegend, PMab-1), Streptavidin (Thermo Fisher Scientific, 12–4317), TCR Vβ (BD Biosciences, 557004), TCRγδ (Thermo Fisher Scientific, GL3), TER-119 (BioLegend, TER-119), TNF-α (Thermo Fisher Scientific, MP6-XT22), UEA-1 (Vector Labs, B-1065), and Zombie Aqua Fixable Viability Dye (BioLegend, 423101).

Immunizations

Antigen-specific T cell responses were studied by immunizing 8- to 12-week-old mice intraperitoneally with 10 μg of TNP-KLH (Biosearch Technologies), 25 μg of TNP-LPS (Biosearch Technologies), or 50 μg of OVA emulsified in Alhydrogel (InvivoGen), boosting with antigen on day 14, and samples were harvested on day 21. Epicutaneous sensitization with OVA was performed as previously described (85).

Protein and antibody assays

Serum samples were analyzed for insulin levels (Thermo Fisher Scientific) LDH (Sigma-Aldrich) at 26 weeks of age. T cell and splenocyte cultures were analyzed for IL-2, IL-4, IL-13, IL-17A, or IFN-γ (BioLegend). Supernatants from B cell cultures and serum were analyzed for total IgM, IgG, or IgA secretion (Southern Biotech). Serum samples from mice, which were immunized with either TNP-LPS or TNP-KLH, were analyzed for TNP-specific antibodies. Serum samples were added to plates coated with TNP(25)-BSA (10 μg/ml) (Biosearch Technologies).

Skin and thymic stromal cell preparation

Skin pieces (1 cm^2) from mice were harvested and finely chopped using scissors after fat removal. They were then digested for 90 min in the media containing liberase (0.25 mg/ml, Roche) and deoxyribonuclease (DNase) II (0.2 mg/ml, Sigma-Aldrich) with continuous shaking at 37°C. Digested skin homogenates were filtered, washed, and resuspended in PBS and used for flow cytometry. For thymic stromal cells, thymic lobes were dissected and then digested for six 5-min rounds in a digestion mix [Liberase (2.5 mg/ml, Roche) and DNase I (10 mg/ml, Sigma-Aldrich)] at 37°C. After each incubation, the thymic lobes were dissociated with pipetting, and after settling, the supernatants from each digest were collected. The supernatant was then centrifuged and passed through a 70-μm filter and prepared for FACS or cell sorting.

S. aureus cutaneous infection

S. aureus skin infection was performed as previously described (86). Briefly, *S. aureus* USA300 SF8300 (MRSA) was prepared for cutaneous infection. Eighteen hours after tape stripping, 10^8 CFU of *S. aureus* in 50 ml of PBS was applied to EC sensitized skin. Mice were analyzed 72 hours later. To enumerate the bacterial load in vivo, *S. aureus* was leveled with PSVue794 reagent kit (LI-COR), following the manufacturer's instructions. PSVue794 fluorescence was quantified at different time points using Pearl Trilogy Small Animal Imaging System (LI-COR). The bacterial load from the cutaneous infected skin was enumerated using two 8-mm^2 skin biopsies. After mechanical homogenization of skin

biopsies, serial dilutions of skin homogenates were cultured on CHROMagar plates for overnight. *S. aureus* was quantified by counting only pink-colored colonies.

TCRVβ CDR3 sequencing

A total of 200,000 M2 thymocytes ($CD4^+CD8^-TCR\beta^{hi}CCR7^+$ $MHCI^+CD69^-CD25^-$) were sorted from mutants and WT control mice. Cells were sent to iRepertoire (Huntsville, AL) where mRNA was extracted and a two-part amplicon-rescued multiplex (arm) PCR amplification of the TCR Vβ genes was performed. These products were pooled and sequenced using the MiSeq 500 cycle kit (~800,000 reads per sample) (iRepertoire). Data analysis was performed using web tools provided by iRepertoire. The hydrophobicity index of CDR3 P6-P7 doublets was determined by calculating the percent of P6-P7 doublets that were considered to promote self-reactivity as previously described (49).

Transcriptome analysis

RNA was purified from sorted mFb or capFb using the RNeasy Mini Kit (Qiagen). cDNA was then synthesized from 10 ng of total RNA using the SuperScript VILO cDNA Synthesis Kit (Thermo Fisher Scientific). Barcoded libraries were prepared using the Ion AmpliSeq Transcriptome Mouse Gene Expression Kit as per the manufacturer's protocol and sequenced using an Ion S5 system (Thermo Fisher Scientific).

Preparation of organ homogenates

Organs were dissected and finely minced. They were then digested in collagenase (2 mg/ml) for 30 min at 37°C with shaking. The digested organs were then passed through a 70-μm filter and washed before staining.

Tissue immunofluorescence

Reagents and mAbs for immunofluorescence were used as described by the manufacturer: streptavidin (BioLegend, 405207) and mAbs to AIRE (Thermo Fisher Scientific, 5H12), B220 (BioLegend, RA3–6B2), CD169 (MOMA-1) (BioLegend, 3D6.112), CD3 (BioLegend, 100240), CD4 (BioLegend, RM4–4), Cleaved Caspase-3 (Cell Signaling Technology, Asp175), FDC-M2 (ImmunoK, FDC-M2), GL7 (BioLegend, GL7), IgD (BioLegend, 11–26c), IgM (Thermo Fisher Scientific, II/41), Madcam1 (BioLegend, MECA-367), RIP3 (Cell Signaling Technology, D4G2A), and UEA-1 (Vector Labs, B-1065). Primary antibodies were diluted in 1× PBS/1% BSA/0.3% Triton X-100 and were incubated with samples overnight at 4°C. Samples were then incubated with fluorescent secondary antibodies for 2 hours at room temperature and imaged (Zeiss, LSM800, or Thermo Fisher Scientific, EVOS M7000). IHC for CD3 in pancreas, lung, and liver was performed by the specialized histopathology core at Brigham and Women's Hospital (Boston, MA).

Blood chemistry

Whole blood was used on the VetScan VS2 Chemistry Analyzer with the comprehensive diagnosis rotor (Abaxis) to measure amylase, ALT, and albumin.

Statistical analysis

All mouse experiments were performed using randomly assigned mice without investigator blinding. All data are presented as mean ± SE. Statistical significance for single comparisons was calculated using the two-sided Student's *t* test or Gehan-Breslow-Wilcoxon test (GraphPad). Statistical significance for multiple comparisons was computed as specified in the figure legends. $P < 0.05$ was considered significant.

Supplementary Material

Refer to Web version on PubMed Central for supplementary material.

Acknowledgments:

We thank J. Jones and K. Stafstrom for technical assistance.

Funding:

This work was supported by 5K08AI116979-04 (to J.C.), 1R01AI139633-01 (to R.S.G.), and the Perkin Fund.

Data and materials availability:

WES data and TCRVβ sequencing data for this project were deposited to the NCBI Sequence Read Archive under BioProject accession number PRJNA746572. All data needed to evaluate the conclusions in the paper are present in the paper or the Supplementary Materials.

REFERENCES AND NOTES

1. Malhotra D, Fletcher AL, Turley SJ, Stromal and hematopoietic cells in secondary lymphoid organs: Partners in immunity. Immunol. Rev 251, 160–176 (2013). [PubMed: 23278748]
2. Sun S-C, The noncanonical NF-κB pathway. Immunol. Rev 246, 125–140 (2012). [PubMed: 22435551]
3. Zhang H, Sun S-C, NF-κB in inflammation and renal diseases. Cell Biosci. 5, 63 (2015). [PubMed: 26579219]
4. Hayden MS, Ghosh S, Shared principles in NF-κB signaling. Cell 132, 344–362 (2008). [PubMed: 18267068]
5. Israël A, The IKK complex, a central regulator of NF-κB activation. Cold Spring Harb. Perspect. Biol 2, a000158 (2010). [PubMed: 20300203]
6. Xiao G, Fong A, Sun S-C, Induction of p100 processing by NF-κB-inducing kinase involves docking IκB kinase α (IKKα) to p100 and IKKα-mediated phosphorylation. J. Biol. Chem 279, 30099–30105 (2004). [PubMed: 15140882]
7. Badran YR, Dedeoglu F, Leyva Castillo JM, Bainter W, Ohsumi TK, Bousvaros A, Goldsmith JD, Geha RS, Chou J, Human *RELA* haploinsufficiency results in autosomal-dominant chronic mucocutaneous ulceration. J. Exp. Med 214, 1937–1947 (2017). [PubMed: 28600438]
8. Dejardin E, Droin NM, Delhase M, Haas E, Cao Y, Makris C, Li Z-W, Karin M, Ware CF, Green DR, The lymphotoxin-β receptor induces different patterns of gene expression via two NF-κB pathways. Immunity 17, 525–535 (2002). [PubMed: 12387745]
9. Claudio E, Brown K, Park S, Wang H, Siebenlist U, BAFF-induced NEMO-independent processing of NF-κB2 in maturing B cells. Nat. Immunol 3, 958–965 (2002). [PubMed: 12352969]
10. Kayagaki N, Yan M, Seshasayee D, Wang H, Lee W, French DM, Grewal IS, Cochran AG, Gordon NC, Yin JP, Starovasnik MA, Dixit VM, BAFF/BLyS receptor 3 binds the B cell survival factor

BAFF ligand through a discrete surface loop and promotes processing of NF-kappaB2. Immunity 17, 515–524 (2002). [PubMed: 12387744]

11. Coope HJ, Atkinson PGP, Huhse B, Belich M, Janzen J, Holman MJ, Klaus GGB, Johnston LH, Ley SC, CD40 regulates the processing of NF-κB2 p100 to p52. EMBO J. 21, 5375–5385 (2002). [PubMed: 12374738]
12. Novack DV, Yin L, Hagen-Stapleton A, Schreiber RD, Goeddel DV, Ross FP, Teitelbaum SL, The IκB function of NF-κB2 p100 controls stimulated osteoclastogenesis. J. Exp. Med 198, 771–781 (2003). [PubMed: 12939342]
13. Sun S-C, The non-canonical NF-κB pathway in immunity and inflammation. Nat. Rev. Immunol 17, 545–558 (2017). [PubMed: 28580957]
14. Polley S, Passos DO, Huang DB, Mulero MC, Mazumder A, Biswas T, Verma IM, Lyumkis D, Ghosh G, Structural Basis for the Activation of IKK1/α. Cell Rep. 17, 1907–1914 (2016). [PubMed: 27851956]
15. Yoshioka T, Nishikomori R, Hara J, Okada K, Hashii Y, Okafuji I, Nodomi S, Kawai T, Izawa K, Ohnishi H, Yasumi T, Nakahata T, Heike T, Autosomal dominant anhidrotic ectodermal dysplasia with immunodeficiency caused by a novel NFKBIA mutation, p.Ser36Tyr, presents with mild ectodermal dysplasia and non-infectious systemic inflammation. J. Clin. Immunol 33, 1165–1174 (2013). [PubMed: 23864385]
16. Liu T, Zhang L, Joo D, Sun S-C, NF-κB signaling in inflammation. Signal Transduct. Target. Ther 2, 17023 (2017). [PubMed: 29158945]
17. Courtois G, Smahi A, Reichenbach J, Döffinger R, Cancrini C, Bonnet M, Puel A, Chable-Bessia C, Yamaoka S, Feinberg J, Dupuis-Girod S, Bodemer C, Livadiotti S, Novelli F, Rossi P, Fischer A, Israël A, Munnich A, Deist FL, Casanova J-L, A hypermorphic IκBα mutation is associated with autosomal dominant anhidrotic ectodermal dysplasia and T cell immunodeficiency. J. Clin. Invest 112, 1108–1115 (2003). [PubMed: 14523047]
18. Döffinger R, Smahi A, Bessia C, Geissmann F, Feinberg J, Durandy A, Bodemer C, Kenwrick S, Dupuis-Girod S, Blanche S, Wood P, Rabia SH, Headon DJ, Overbeek PA, Deist FL, Holland SM, Belani K, Kumararatne DS, Fischer A, Shapiro R, Conley ME, Reimund E, Kalhoff H, Abinun M, Munnich A, Israël A, Courtois G, Casanova J-L, X-linked anhidrotic ectodermal dysplasia with immunodeficiency is caused by impaired NF-κB signaling. Nat. Genet 27, 277–285 (2001). [PubMed: 11242109]
19. Merico D, Sharfe N, Hu P, Herbrick J-A, Roifman CM, RelB deficiency causes combined immunodeficiency. LymphoSign J. 2, 147–155 (2015).
20. Chen K, Coonrod EM, Kumánovics A, Franks ZF, Durtschi JD, Margraf RL, Wu W, Heikal NM, Augustine NH, Ridge PG, Hill HR, Jorde LB, Weyrich AS, Zimmerman GA, Gundlapalli AV, Bohnsack JF, Voelkerding KV, Germline mutations in NFKB2 implicate the noncanonical NF-κB pathway in the pathogenesis of common variable immunodeficiency. Am. J. Hum. Genet 93, 812–824 (2013). [PubMed: 24140114]
21. Willmann KL, Klaver S, Doğu F, Santos-Valente E, Garncarz W, Bilic I, Mace E, Salzer E, Domínguez Conde C, Sic H, Májek P, Banerjee PP, Vladimer GI, Haskoloğlu Ş, Gökalp Bolkent M, Küpesiz A, Condino-Neto A, Colinge J, Superti-Furga G, Pickl WF, van Zelm MC, Eibel H, Orange JS, Ikincioğulları A, Boztuğ K, Biallelic loss-of-function mutation in *NIK* causes a primary immunodeficiency with multifaceted aberrant lymphoid immunity. Nat. Commun 5, 5360 (2014). [PubMed: 25406581]
22. Beaussant-Cohen S, Jaber F, Massaad MJ, Weeks S, Jones J, Alosaimi MF, Wallace J, Al-Herz W, Geha RS, Chou J, Combined immunodeficiency in a patient with c-Rel deficiency. J. Allergy Clin. Immunol 144, 606–608.e4 (2019). [PubMed: 31103457]
23. Lahtela J, Nousiainen HO, Stefanovic V, Tallila J, Viskari H, Karikoski R, Gentile M, Saloranta C, Varilo T, Salonen R, Kestilä M, Mutant CHUK and severe fetal encasement malformation. N. Engl. J. Med 363, 1631–1637 (2010). [PubMed: 20961246]
24. Hu Y, Baud V, Oga T, Kim KI, Yoshida K, Karin M, IKKα controls formation of the epidermis independently of NF-kappaB. Nature 410, 710–714 (2001). [PubMed: 11287960]
25. Sil AK, Maeda S, Sano Y, Roop DR, Karin M, IκB kinase-α acts in the epidermis to control skeletal and craniofacial morphogenesis. Nature 428, 660–664 (2004). [PubMed: 15071597]

26. Takeda K, Takeuchi O, Tsujimura T, Itami S, Adachi O, Kawai T, Sanjo H, Yoshikawa K, Terada N, Akira S, Limb and skin abnormalities in mice lacking IKKα. Science 284, 313–316 (1999). [PubMed: 10195895]
27. Li Q, Lu Q, Hwang JY, Buscher D, Lee K-F, Izpisua-Belmonte JC, Verma IM, IKK1-deficient mice exhibit abnormal development of skin and skeleton. Genes Dev. 13, 1322–1328 (1999). [PubMed: 10346820]
28. Descargues P, Sil AK, Karin M, IKKalpha, a critical regulator of epidermal differentiation and a suppressor of skin cancer. EMBO J. 27, 2639–2647 (2008). [PubMed: 18818691]
29. Descargues P, Sil AK, Sano Y, Korchynskyi O, Han G, Owens P, Wang X-J, Karin M, IKKα is a critical coregulator of a Smad4-independent TGFβ-Smad2/3 signaling pathway that controls keratinocyte differentiation. Proc. Natl. Acad. Sci. U.S.A 105, 2487–2492 (2008). [PubMed: 18268325]
30. Penzo M, Habiel DM, Ramadass M, Kew RR, Marcu KB, Cell migration to CXCL12 requires simultaneous IKKα and IKKβ-dependent NF-κB signaling. Biochim. Biophys. Acta 1843, 1796–1804 (2014). [PubMed: 24747690]
31. Suto H, Katakai T, Sugai M, Kinashi T, Shimizu A, CXCL13 production by an established lymph node stromal cell line via lymphotoxin-beta receptor engagement involves the cooperation of multiple signaling pathways. Int. Immunol 21, 467–476 (2009). [PubMed: 19251935]
32. Gardam S, Brink R, Non-canonical NF-κB signaling initiated by BAFF influences B cell biology at multiple junctures. Front. Immunol 4, 509 (2014). [PubMed: 24432023]
33. Yan M, Brady JR, Chan B, Lee WP, Hsu B, Harless S, Cancro M, Grewal IS, Dixit VM, Identification of a novel receptor for B lymphocyte stimulator that is mutated in a mouse strain with severe B cell deficiency. Curr. Biol 11, 1547–1552 (2001). [PubMed: 11591325]
34. Smulski CR, Eibel H, BAFF and BAFF-receptor in B cell selection and survival. Front. Immunol 9, 2285 (2018). [PubMed: 30349534]
35. Barber CL, Montecino-Rodriguez E, Dorshkind K, Reduced production of B-1-specified common lymphoid progenitors results in diminished potential of adult marrow to generate B-1 cells. Proc. Natl. Acad. Sci. U.S.A 108, 13700–13704 (2011). [PubMed: 21808010]
36. Sage PT, Alvarez D, Godec J, von Andrian UH, Sharpe AH, Circulating T follicular regulatory and helper cells have memory-like properties. J. Clin. Invest 124, 5191–5204 (2014). [PubMed: 25347469]
37. Pfaff CM, Marquardt Y, Fietkau K, Baron JM, Lüscher B, The psoriasis-associated IL-17A induces and cooperates with IL-36 cytokines to control keratinocyte differentiation and function. Sci. Rep 7, 15631 (2017). [PubMed: 29142248]
38. Cho JS, Pietras EM, Garcia NC, Ramos RI, Farzam DM, Monroe HR, Magorien JE, Blauvelt A, Kolls JK, Cheung AL, Cheng G, Modlin RL, Miller LS, IL-17 is essential for host defense against cutaneous Staphylococcus aureus infection in mice. J. Clin. Invest 120, 1762–1773 (2010). [PubMed: 20364087]
39. Li L, Ruan Q, Hilliard B, DeVirgiliis J, Karin M, Chen YH, Transcriptional regulation of the Th17 immune response by IKKα. J. Exp. Med 208, 787–796 (2011). [PubMed: 21402739]
40. Jin W, Zhou XF, Yu J, Cheng X, Sun SC, Regulation of Th17 cell differentiation and EAE induction by MAP3K NIK. Blood 113, 6603–6610 (2009). [PubMed: 19411637]
41. Kinoshita D, Hirota F, Kaisho T, Kasai M, Izumi K, Bando Y, Mouri Y, Matsushima A, Niki S, Han H, Oshikawa K, Kuroda N, Maegawa M, Irahara M, Takeda K, Akira S, Matsumoto M, Essential role of IκB kinase alpha in thymic organogenesis required for the establishment of self-tolerance. J. Immunol 176, 3995–4002 (2006). [PubMed: 16547234]
42. Boehm S, P2Ys go neuronal: Modulation of Ca^{2+} and K^{+} channels by recombinant receptors. Br. J. Pharmacol 138, 1–3 (2003). [PubMed: 12522065]
43. Shen H, Ji Y, Xiong Y, Kim H, Zhong X, Jin MG, Shah YM, Omary MB, Liu Y, Qi L, Rui L, Medullary thymic epithelial NF-kB-inducing kinase (NIK)/IKKα pathway shapes autoimmunity and liver and lung homeostasis in mice. Proc. Natl. Acad. Sci. U.S.A 116, 19090–19097 (2019). [PubMed: 31481626]

44. Nitta T, Tsutsumi M, Nitta S, Muro R, Suzuki EC, Nakano K, Tomofuji Y, Sawa S, Okamura T, Penninger JM, Takayanagi H, Fibroblasts as a source of self-antigens for central immune tolerance. Nat. Immunol 21, 1172–1180 (2020). [PubMed: 32839611]
45. Daley SR, Hu DY, Goodnow CC, Helios marks strongly autoreactive $CD4^+$ T cells in two major waves of thymic deletion distinguished by induction of PD-1 or NF-κB. J. Exp. Med 210, 269–285 (2013). [PubMed: 23337809]
46. Barthlott T, Kohler H, Eichmann K, Asynchronous coreceptor downregulation after positive thymic selection: Prolonged maintenance of the double positive state in CD8 lineage differentiation due to sustained biosynthesis of the CD4 coreceptor. J. Exp. Med 185, 357–362 (1997). [PubMed: 9016884]
47. James KD, Jenkinson WE, Anderson G, T-cell egress from the thymus: Should I stay or should I go? J. Leukoc. Biol 104, 275–284 (2018). [PubMed: 29485734]
48. Baran-Gale J, Morgan MD, Maio S, Dhalla F, Calvo-Asensio I, Deadman ME, Handel AE, Maynard A, Chen S, Green F, Sit RV, Neff NF, Darmanis S, Tan W, May AP, Marioni JC, Ponting CP, Holländer GA, Ageing compromises mouse thymus function and remodels epithelial cell differentiation. eLife 9, e56221 (2020). [PubMed: 32840480]
49. Stadinski BD, Shekhar K, Gómez-Touriño I, Jung J, Sasaki K, Sewell AK, Peakman M, Chakraborty AK, Huseby ES, Hydrophobic CDR3 residues promote the development of self-reactive T cells. Nat. Immunol 17, 946–955 (2016). [PubMed: 27348411]
50. Hu J, Zhai C, Hu J, Li Z, Fei H, Wang Z, Fan W, MiR-23a inhibited IL-17-mediated proinflammatory mediators expression via targeting IKKα in articular chondrocytes. Int. Immunopharmacol 43, 1–6 (2017). [PubMed: 27936459]
51. Eden K, Rothschild DE, McDaniel DK, Heid B, Allen IC, Noncanonical NF-κB signaling and the essential kinase NIK modulate crucial features associated with eosinophilic esophagitis pathogenesis. Dis. Model. Mech 10, 1517–1527 (2017). [PubMed: 29259025]
52. Gareus R, Huth M, Breiden B, Nenci A, Rösch N, Haase I, Bloch W, Sandhoff K, Pasparakis M, Normal epidermal differentiation but impaired skin-barrier formation upon keratinocyte-restricted IKK1 ablation. Nat. Cell Biol 9, 461–469 (2007). [PubMed: 17351639]
53. Platsidaki E, Kouris A, Agiasofitou E, Antoniou C, Kontochristopoulos G, Periorbital hyperpigmentation in patients with xanthelasma palpebrarum: An interesting observation. J. Clin. Aesthet. Dermatol 9, 52–54 (2016). [PubMed: 27721911]
54. Giacomin PR, Moy RH, Noti M, Osborne LC, Siracusa MC, Alenghat T, Liu B, McCorkell KA, Troy AE, Rak GD, Hu Y, May MJ, Ma HL, Fouser LA, Sonnenberg GF, Artis D, Epithelial-intrinsic IKKα expression regulates group 3 innate lymphoid cell responses and antibacterial immunity. J. Exp. Med 212, 1513–1528 (2015). [PubMed: 26371187]
55. Eftychi C, Pasparakis M, Epithelial IKKα licenses ILC3s to defend the intestinal barrier. J. Exp. Med 212, 1483 (2015). [PubMed: 26392427]
56. Onder L, Mörbe U, Pikor N, Novkovic M, Cheng H-W, Hehlgans T, Pfeffer K, Becher B, Waisman A, Rülicke T, Gommerman J, Mueller CG, Sawa S, Scandella E, Ludewig B, Lymphatic endothelial cells control initiation of lymph node organogenesis. Immunity 47, 80–92.e4 (2017). [PubMed: 28709801]
57. van de Pavert SA, Mebius RE, New insights into the development of lymphoid tissues. Nat. Rev. Immunol 10, 664–674 (2010). [PubMed: 20706277]
58. Katakam AK, Brightbill H, Franci C, Kung C, Nunez V, Jones C III, Peng I, Jeet S, Wu LC, Mellman I, Delamarre L, Austin CD, Dendritic cells require NIK for CD40-dependent cross-priming of $CD8^+$ T cells. Proc. Natl. Acad. Sci. U.S.A 112, 14664–14669 (2015). [PubMed: 26561586]
59. Hofmann J, Mair F, Greter M, Schmidt-Supprian M, Becher B, NIK signaling in dendritic cells but not in T cells is required for the development of effector T cells and cell-mediated immune responses. J. Exp. Med 208, 1917–1929 (2011). [PubMed: 21807870]
60. Hofmann J, Greter M, Du Pasquier L, Becher B, B-cells need a proper house, whereas T-cells are happy in a cave: The dependence of lymphocytes on secondary lymphoid tissues during evolution. Trends Immunol. 31, 144–153 (2010). [PubMed: 20181529]

61. Piccolella E, Spadaro F, Ramoni C, Marinari B, Costanzo A, Levrero M, Thomson L, Abraham RT, Tuosto L, Vav-1 and the IKKα subunit of I κB kinase functionally associate to induce NF-κB activation in response to CD28 engagement. J. Immunol 170, 2895–2903 (2003). [PubMed: 12626540]
62. Mills DM, Bonizzi G, Karin M, Rickert RC, Regulation of late B cell differentiation by intrinsic IKKα-dependent signals. Proc. Natl. Acad. Sci. U.S.A 104, 6359–6364 (2007). [PubMed: 17404218]
63. Brightbill HD, Jackman JK, Suto E, Kennedy H, Jones III C, Chalasani S, Lin Z, Tam L, Roose-Girma M, Balazs M, Austin CD, Lee WP, Wu LC, Conditional Deletion of NF-κB–inducing kinase (NIK) in adult mice disrupts mature B cell survival and activation. J. Immunol 195, 953–964 (2015). [PubMed: 26116508]
64. Miyawaki S, Nakamura Y, Suzuka H, Koba M, Shibata Y, Yasumizu R, Ikehara S, A new mutation, aly, that induces a generalized lack of lymph nodes accompanied by immunodeficiency in mice. Eur. J. Immunol 24, 429–434 (1994). [PubMed: 8299692]
65. Koike R, Nishimura T, Yasumizu R, Tanaka H, Hataba Y, Hataba Y, Watanabe T, Miyawaki S, Miyasaka M, The splenic marginal zone is absent in alymphoplastic aly mutant mice. Eur. J. Immunol 26, 669–675 (1996). [PubMed: 8605936]
66. Shinkura R, Kitada K, Matsuda F, Tashiro K, Ikuta K, Suzuki M, Kogishi K, Serikawa T, Honjo T, Alymphoplasia is caused by a point mutation in the mouse gene encoding Nf-κb-inducing kinase. Nat. Genet 22, 74–77 (1999). [PubMed: 10319865]
67. Mebius RE, Organogenesis of lymphoid tissues. Nat. Rev. Immunol 3, 292–303 (2003). [PubMed: 12669020]
68. Paxian S, Merkle H, Riemann M, Wilda M, Adler G, Hameister H, Liptay S, Pfeffer K, Schmid RM, Abnormal organogenesis of Peyer's patches in mice deficient for NF-κB1, NF-κB2, and Bcl-3. Gastroenterology 122, 1853–1868 (2002). [PubMed: 12055593]
69. Hayden MS, Ghosh S, NF-κB in immunobiology. Cell Res. 21, 223–244 (2011). [PubMed: 21243012]
70. Hoffman W, Lakkis FG, Chalasani G, B Cells, Antibodies, and More. Clin. J. Am. Soc. Nephrol 11, 137–154 (2016). [PubMed: 26700440]
71. Boehm T, Scheu S, Pfeffer K, Bleul CC, Thymic medullary epithelial cell differentiation, thymocyte emigration, and the control of autoimmunity require lympho-epithelial cross talk via LTbetaR. J. Exp. Med 198, 757–769 (2003). [PubMed: 12953095]
72. Takaba H, Morishita Y, Tomofuji Y, Danks L, Nitta T, Komatsu N, Kodama T, Takayanagi H, Fezf2 orchestrates a thymic program of self-antigen expression for immune tolerance. Cell 163, 975–987 (2015). [PubMed: 26544942]
73. Zhu M, Fu YX, Coordinating development of medullary thymic epithelial cells. Immunity 29, 386–388 (2008). [PubMed: 18799147]
74. Aschenbrenner K, D'Cruz LM, Vollmann EH, Hinterberger M, Emmerich J, Swee LK, Rolink A, Klein L, Selection of Foxp3^{+} regulatory T cells specific for self antigen expressed and presented by Aire^{+} medullary thymic epithelial cells. Nat. Immunol 8, 351–358 (2007). [PubMed: 17322887]
75. Klein L, Kyewski B, Allen PM, Hogquist KA, Positive and negative selection of the T cell repertoire: What thymocytes see (and don't see). Nat. Rev. Immunol 14, 377–391 (2014). [PubMed: 24830344]
76. Wirasinha RC, Davies AR, Srivastava M, Sheridan JM, Sng XYX, Delmonte OM, Dobbs K, Loh KL, Miosge LA, Lee CE, Chand R, Chan A, Yap JY, Keller MD, Chen K, Rossjohn J, la Gruta NL, Vinuesa CG, Reid HH, Lionakis MS, Notarangelo LD, Gray DHD, Goodnow CC, Cook MC, Daley SR, *Nfkb2* variants reveal a p100-degradation threshold that defines autoimmune susceptibility. J. Exp. Med 218, e20200476 (2021). [PubMed: 33107914]
77. Li J, Chen S, Chen W, Ye Q, Dou Y, Xiao Y, Zhang L, Minze LJ, Li XC, Xiao X, Role of the NF-κB family member RelB in regulation of Foxp3^{+} regulatory T cells in vivo. J. Immunol 200, 1325–1334 (2018). [PubMed: 29298831]

78. Weih F, Carrasco D, Durham SK, Barton DS, Rizzo CA, Ryseck R-P, Lira SA, Bravo R, Multiorgan inflammation and hematopoietic abnormalities in mice with a targeted disruption of RelB, a member of the NF-κB/Rel family. Cell 80, 331–340 (1995). [PubMed: 7834753]

79. Akiyama T, Shimo Y, Yanai H, Qin J, Ohshima D, Maruyama Y, Asaumi Y, Kitazawa J, Takayanagi H, Penninger JM, Matsumoto M, Nitta T, Takahama Y, Inoue J-I, The tumor necrosis factor family receptors RANK and CD40 cooperatively establish the thymic medullary microenvironment and self-tolerance. Immunity 29, 423–437 (2008). [PubMed: 18799149]

80. Burkly L, Hession C, Ogata L, Reilly C, Marconl LA, Olson D, Tizard R, Gate R, Lo D, Expression of relB is required for the development of thymic medulla and dendritic cells. Nature 373, 531–536 (1995). [PubMed: 7845467]

81. Miraghazadeh B, Cook MC, Nuclear factor-κB in autoimmunity: Man and mouse. Front. Immunol 9, 613 (2018). [PubMed: 29686669]

82. Hacker H, Chi L, Rehg JE, Redecke V, NIK prevents the development of hypereosinophilic syndrome-like disease in mice independent of IKKα activation. J. Immunol 188, 4602–4610 (2012). [PubMed: 22474019]

83. Ramakrishnan SK, Zhang H, Ma X, Jung I, Schwartz AJ, Triner D, Devenport SN, Das NK, Xue X, Zeng MY, Hu Y, Mortensen RM, Greenson JK, Cascalho M, Wobus CE, Colacino JA, Nunez G, Rui L, Shah YM, Intestinal non-canonical NFκB signaling shapes the local and systemic immune response. Nat. Commun 10, 660 (2019). [PubMed: 30737385]

84. Jabara HH, Boyden SE, Chou J, Ramesh N, Massaad MJ, Benson H, Bainter W, Fraulino D, Rahimov F, Sieff C, Liu Z-J, Alshemmari SH, Al-Ramadi BK, Al-Dhekri H, Arnaout R, Abu-Shukair M, Vatsayan A, Silver E, Ahuja S, Davies EG, Sola-Visner M, Ohsumi TK, Andrews NC, Notarangelo LD, Fleming MD, Al-Herz W, Kunkel LM, Geha RS, A missense mutation in *TFRC*, encoding transferrin receptor 1, causes combined immunodeficiency. Nat. Genet 48, 74–78 (2016). [PubMed: 26642240]

85. He R, Oyoshi MK, Jin H, Geha RS, Epicutaneous antigen exposure induces a Th17 response that drives airway inflammation after inhalation challenge. Proc. Natl. Acad. Sci. U.S.A 104, 15817–15822 (2007). [PubMed: 17893340]

86. Leyva-Castillo J-M, McGurk A, Geha MDR, Allergic skin inflammation and S. *aureus* skin colonization are mutually reinforcing. Clin. Immunol 218, 108511 (2020). [PubMed: 32569845]

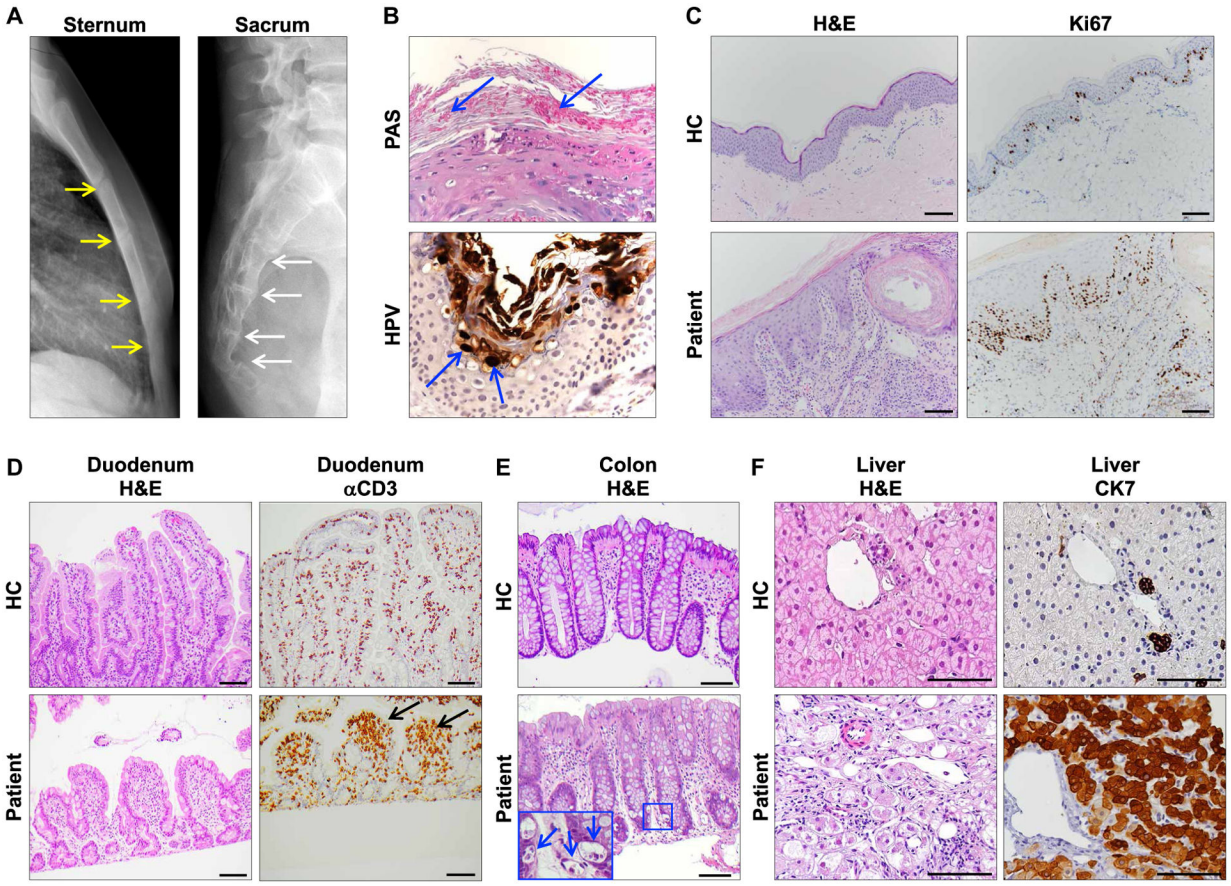

Fig. 1. Skeletal, skin, and organ abnormalities in the patient.

(**A**) Radiographs of the chest and sacrum of the patient at age 18. Arrows indicate incomplete bone fusion in the sternum and sacrum. (**B**) Top: Patient lesional skin stained with periodic acid–Schiff (PAS). Arrows indicate the presence of fungal elements. Bottom: IHC staining of patient lesional skin for HPV. Arrows indicate foci of intranuclear immunoreactivity for HPV protein. (**C**) H&E staining and IHC staining for Ki67 of nonlesional skin from the patient and skin from a HC. Scale bars, 200 μm. The H&E-stained sections demonstrate epidermal thickening and hyperkeratosis as well as increased Ki67 labeling within the basal and suprabasal layers in the patient compared with control. (**D**) Duodenal biopsies from patient and HC stained with H&E and for $CD3^+$ cells by IHC. Arrows point to collections of $CD3^+$ cells in the patient. Scale bars, 100 μm. (**E**) Colon biopsies from patient and HC stained with H&E. The inset shows apoptotic bodies indicated by arrows. Scale bars, 100 μm. (**F**) Liver biopsies from patient and HC stained with H&E (left) and for CK7 by IHC (right). Scale bars, 200 μm.

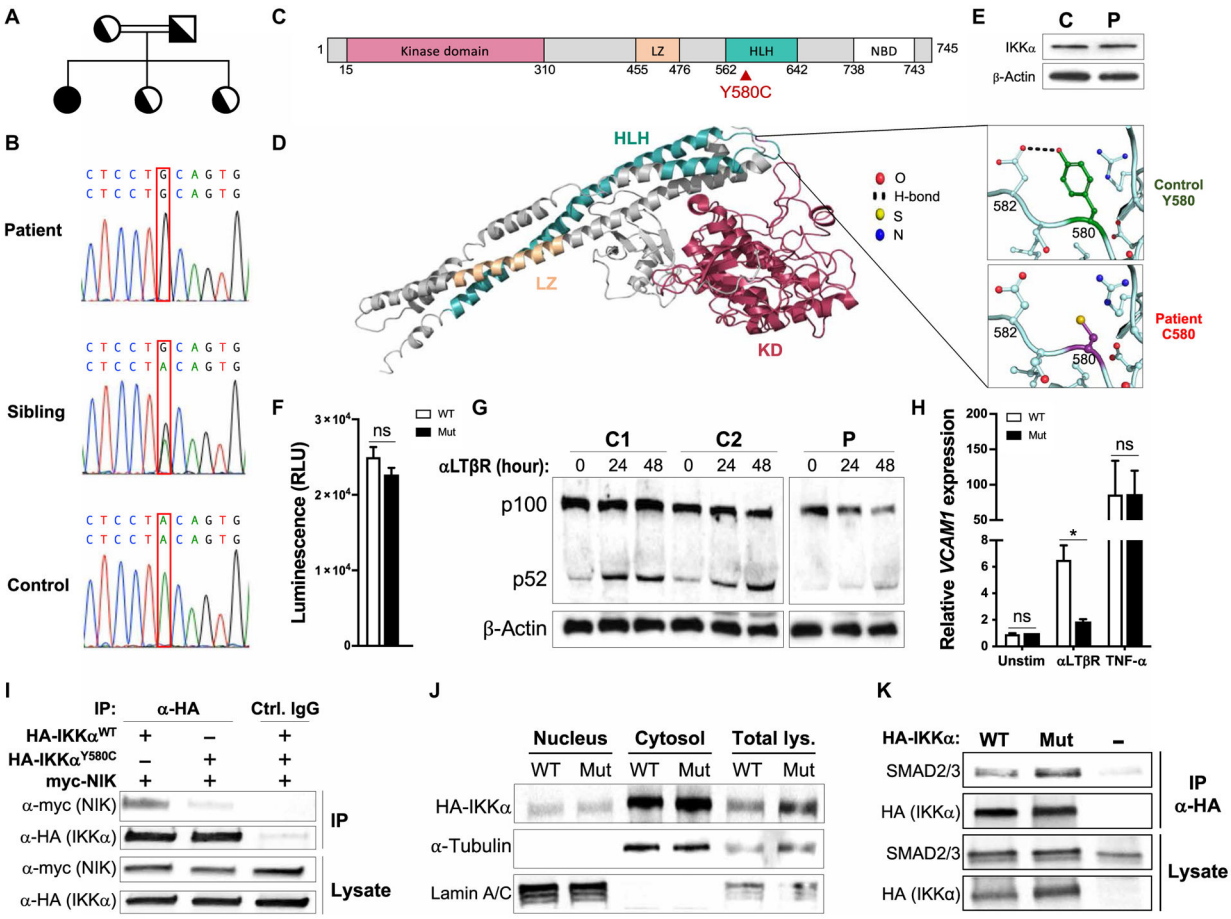

Fig. 2. Effect of the Y580C mutation on IKKα expression and function.

(**A**) Family pedigree. (**B**) Sanger sequencing of the c.A1739G *CHUK* variant. (**C**) Linear map of IKKα with the location of the Y580C mutation. LZ, leucine zipper; NBD, NEMO-binding domain. (**D**) Ribbon diagram of IKKα. Insets show the potential impact of the Y580C mutation on hydrogen bond formation with neighboring residue D582. KD, kinase domain. (**E**) IKKα immunoblot in patient and control fibroblasts. (**F**) IKKα kinase activity of mutant and WT IKKα against $I\kappa B\alpha_{21–41}$ substrate measured by ADP-Glo kinase assay. RLU, relative light unit. (**G** and **H**) Immunoblot of p100 and p52 after anti-LTβR stimulation (G) and *VCAM1* mRNA levels after anti-LTβR or TNF-α stimulation (H) of patient (P) and two control (C1 and C2) fibroblasts. (**I**) Coimmunoprecipitation of Myc-NIK with HA-IKKα and HA-$IKK\alpha^{Y580C}$ (top) and immunoblots of lysates (bottom) of HEK293T transfectants. IP, immunoprecipitation. (**J**) Anti-HA (IKKα) immunoblots of nuclear extracts, cytoplasmic extracts, and lysates of HEK293T transfectants. α-Tubulin and lamin A/C immunoblots are used to monitor the purity of the nuclear and cytoplasmic fractions. (**K**) Coimmunoprecipitation of SMAD2 and SMAD3 with HA-tagged WT or $IKK\alpha^{Y580C}$ (top) and immunoblots of lysates (bottom). SMAD2 and SMAD3 comigrate and are recognized by the same antibody. Similar results were obtained in two other independent experiments in (E) to (K). Columns and bars in (F) and (H) represent mean and SEM of three independent experiments. $^*P \leq 0.05$; ns, not significant by two-tailed Student's *t* test.

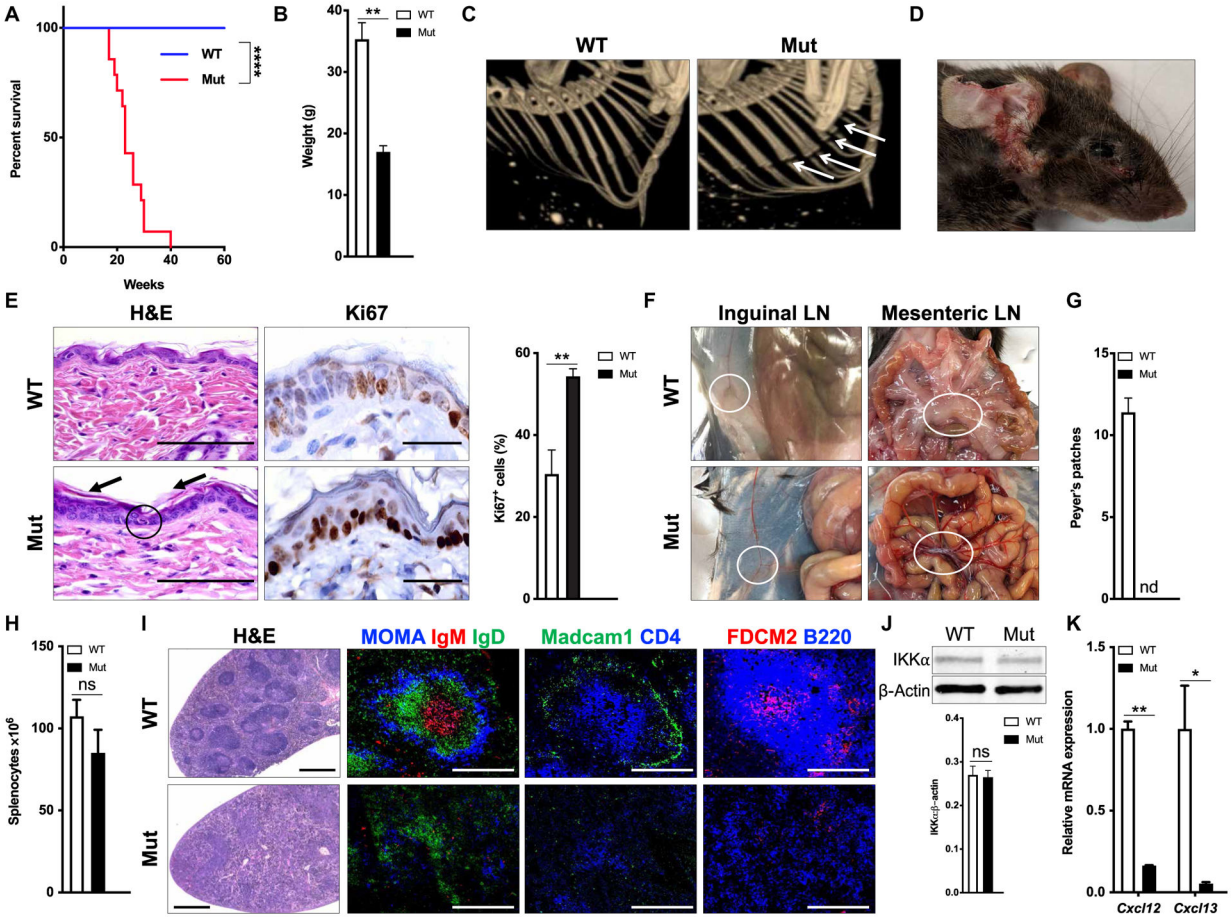

Fig. 3. IKKα mutant mice die early, lack lymph nodes, and have disorganized splenic architecture.

(**A**) Survival curve of mutant mice ($n = 16$) and WT controls ($n = 16$ per genotype). (**B**) Weight of mutant mice and WT controls at 26 weeks ($n = 3$ per genotype). (**C**) Representative computerized tomography scan of chest in mutant and WT control. Arrows indicate the absence of rib bone fusion. (**D**) Photograph of a 26-week-old mutant mouse depicting conjunctivitis and auricular and post-auricular ulcerating skin lesion. (**E**) H&E staining (left) and IHC staining for Ki67 (right) with quantitation of nonlesional skin from WT and mutant mice showing mild epidermal thickening (encircled) and hyperkeratosis (arrows) as well as increased Ki67 staining within the basal cell layer in the mutant animals. Scale bars, 100 μm. (**F**) Absence of inguinal LNs (left) and mesenteric LNs (right) in a mutant and WT mouse. (**G**) Numbers of Peyer's patches in the ileum ($n = 5$ per genotype). nd, not detected. (**H**) Splenocyte numbers in 8- to 12-week-old mice ($n = 5$ per genotype). (**I**) Representative photomicrograph of spleen sections stained with H&E (first) or by immunofluorescence for MOMA, IgM, and IgD (second), Madcam1 and CD4 (third), and FDCM2 and B220 (fourth). Scale bars, 100 μm. (**J**) Representative immunoblot of IKKα in splenocyte lysates from mutant and WT control and quantitation of IKKα expression ($n = 3$ per genotype). (**K**) *Cxcl12* and *Cxcl13* mRNA expression by splenocytes from mutants and WT controls ($n = 3$ per genotype). Similar results were obtained with three mice per genotype in (C), (E), (F), and (I). Columns and bars in (B), (G), (H), (J), and (K) represent

mean and SEM. ****$P \leq 0.0001$ by Gehan-Breslow-Wilcoxon test in (A). *$P \leq 0.05$ and *$P \leq 0.01$ by two-tailed Student's t test in (B), (G), (H), (J), and (K).

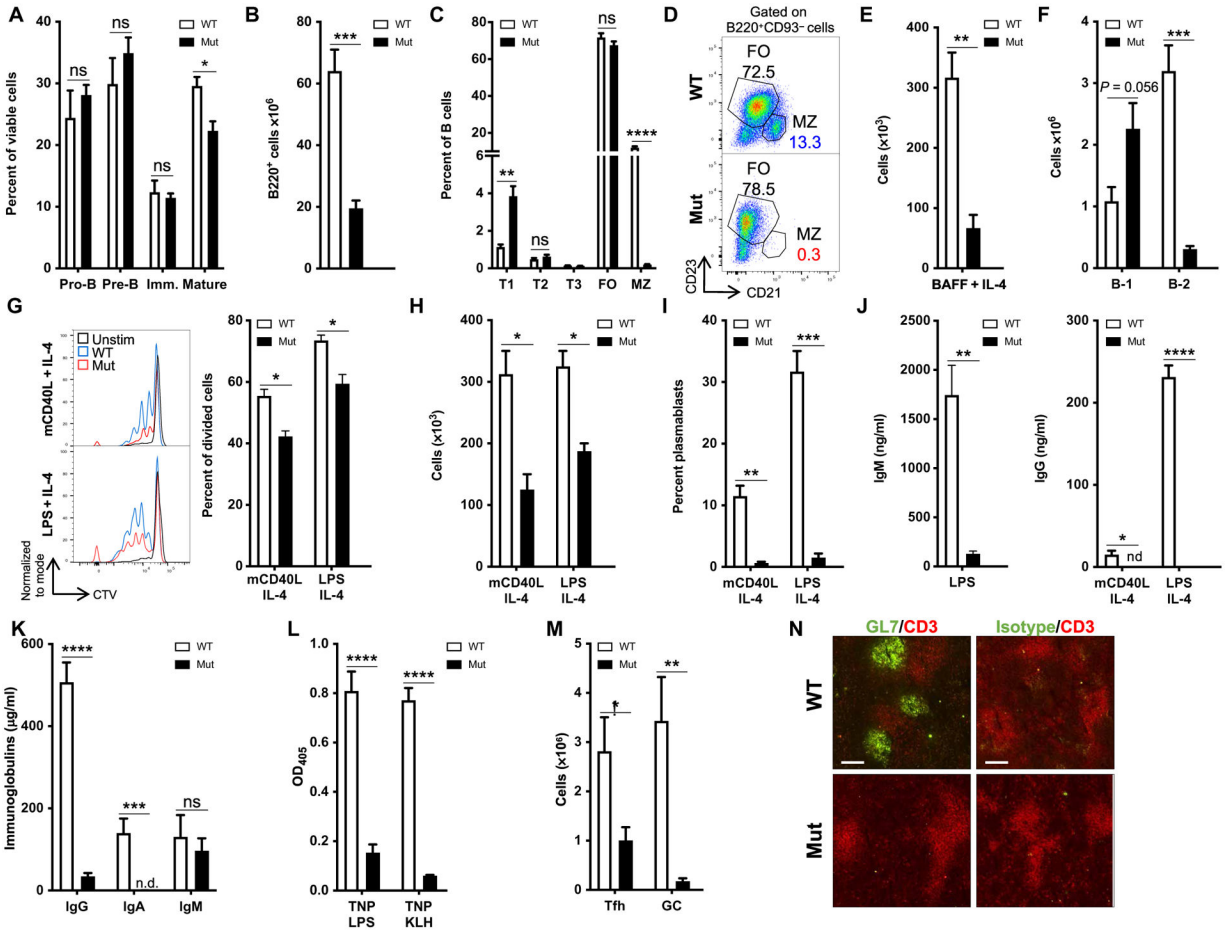

Fig. 4. B cell phenotype and function in IKKα$^{Y580C/Y580C}$ mice.

(**A to D**) B cell subsets in BM (A), splenic B cell number (B) and subsets (C), and representative FACS analysis of splenic FO and MZ B cells (D) in mutant mice ($n = 5$) and WT controls ($n = 4$). FO, follicular. (**E**) Numbers of mutant and WT B cells after culture for 96 hours with rBAFF + IL-4 ($n = 3$ per genotype). (**F**) Distribution of B220^{int}IgM^{+} B-1 and B220^{hi} IgM^{+} B-2 cells among viable peritoneal lymphocytes of mutant mice ($n = 5$) and WT controls ($n = 4$). (**G** to **I**) Representative flow cytometry of CTV dye dilution (G), numbers of FVD^{-} viable cells (H), and percentage of B220^{int}CD138^{+} plasmablasts (I) of mutant and WT B cells stimulated with mCD40L + IL-4 or LPS + IL-4 ($n = 3$ per genotype). (**J**) LPS-driven IgM secretion and LPS + IL-4– and mCD40L + IL-4–driven IgG secretion by mutant and WT B cells ($n = 3$ per genotype). (**K**) Serum IgG, IgA, and IgM levels in mutant mice and WT controls ($n = 6$ per genotype). (**L**) Serum IgG anti-TNP antibody response to TNP-LPS and TNP-KLH immunization in mutants and WT controls ($n = 5$ per genotype). OD_{405}, optical density at 405 nm. (**M**) Numbers of splenic CD4^{+}CXCR5^{+}PD1^{+} T_{FH} cells and B220^{+}FAS^{+}GL7^{+} GC B cells in TNP-KLH–immunized mice ($n = 5$ per genotype). (**N**) Representative immunofluorescence staining for CD3 and GL7 in spleen sections from TNP-KLH–immunized mice. Scale bars, 500 μm. Similar results were obtained in three mice per genotype. Columns and bars represent mean and SEM. *$P \leq 0.05$, **$P \leq 0.01$, ***$P \leq 0.001$, and ****$P \leq 0.0001$ by two-tailed Student's t test.

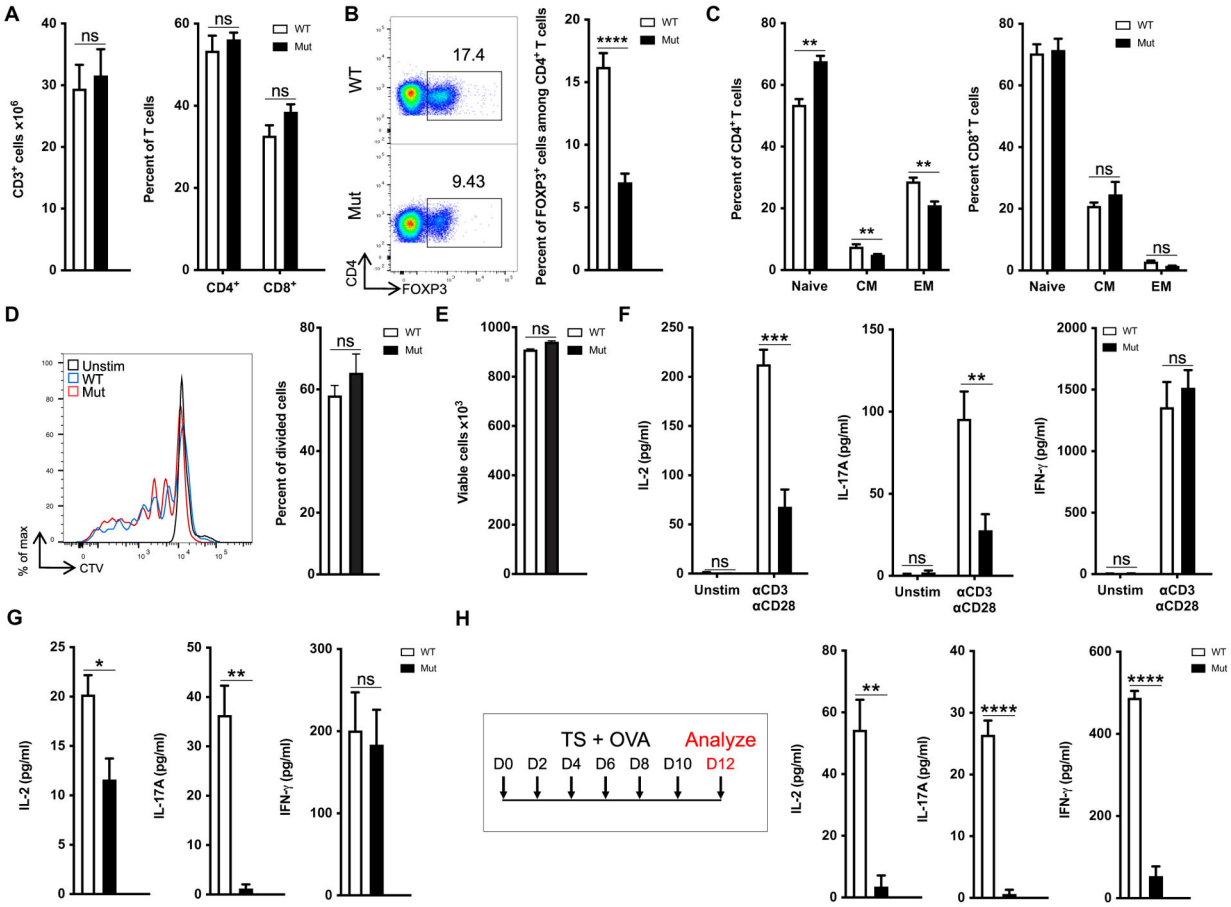

Fig. 5. Impaired IL-2 and IL-17A production by T cells and absent T cell response to cutaneous immunization in IKKα$^{Y580C/Y580C}$ mice.

(**A** and **B**) Number of CD3$^+$ cells and distribution of CD4$^+$ and CD8$^+$ T cells (A), percentage of splenic CD4$^+$FOXP3$^+$ T_{regs} among CD4$^+$ cells (B), and distribution of CD62L^{hi}CD44^{lo} naïve T cells, CD62L^{hi}CD44^{hi} central memory T cells (CM), and CD62L^{low}CD44^{hi} effector memory T cells (EM) among CD4$^+$ and CD8$^+$ T cells (C) in spleens of 8- to 12-week-old mutant mice and WT controls (n = 5 per genotype). (**D** to **F**) Representative histogram of CTV dye dilution and percentage of cells that have undergone cell division (D), number of FVD$^-$ viable cells (E), and secretion of cytokines (F) after αCD3$^+$ αCD28 stimulation for 72 hours of purified splenic T cells from mutant mice (n = 4) and WT controls (n = 3). (**G**) Cytokine secretion by OVA-stimulated splenocytes from intraperitoneally immunized mice (n = 5 per genotype). (**H**) Epicutaneous immunization protocol and cytokine secretion by OVA-stimulated splenocytes from epicutaneously immunized mice (n = 5 per genotype). T/S, tape stripping. Columns and bars represent mean and SEM. *$P \leq 0.05$, *$P \leq 0.01$, ***$P \leq 0.001$, ****$P \leq 0.0001$ by two-tailed Student's t test.

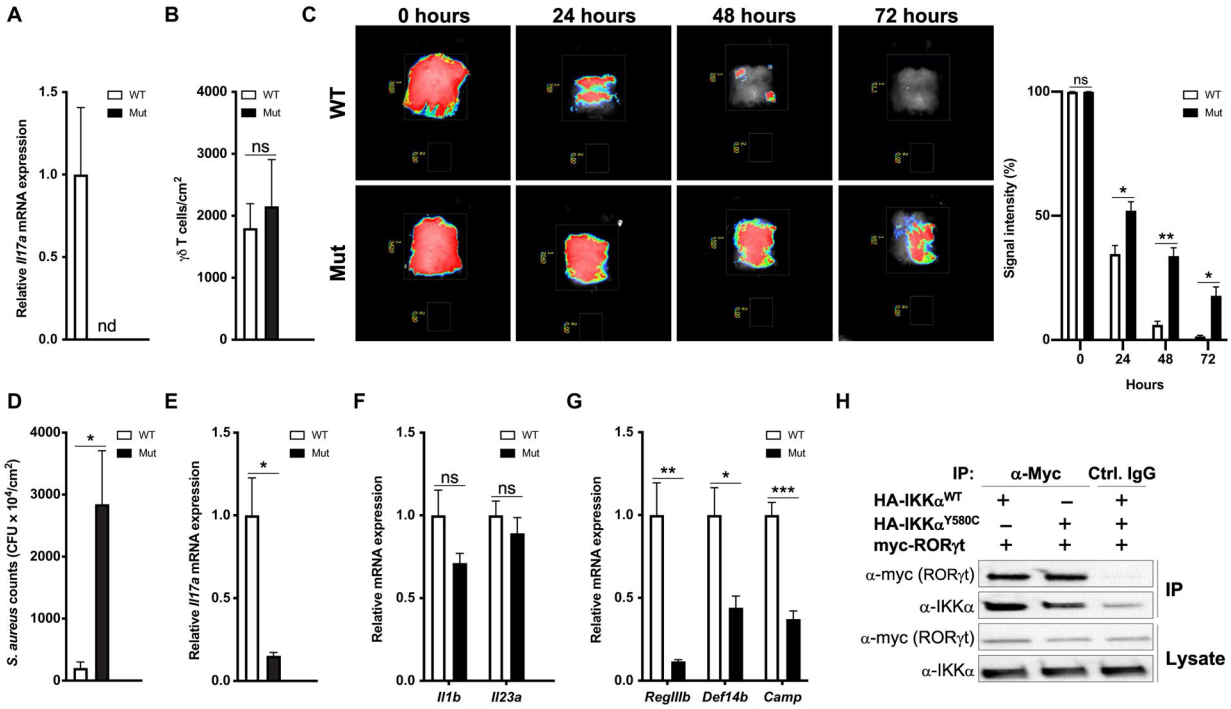

Fig. 6. Reduced cutaneous *Il17a* expression and susceptibility to *S. aureus* skin infection in IKKα$^{Y580C/Y580C}$ mice.

(**A** and **B**) *Il17a* expression (A) and numbers of TCRγδ^{+} cells (B) in the skin of mutants and WT controls. (**C** to **G**) Representative in vivo imaging of *S. aureus* bioluminescence and its quantitation in mice (C), *S. aureus* CFUs in skin homogenates (D), cutaneous expression of *Il17a* (E), *Il1b* and *Il23a (p19)* (F), and AMP genes (G) postinfection of tape stripped skin with PSVue 794–labeled *S. aureus* USA300 strain. Measurements in (D) to (G) were made 72 hours after infection. Results are from two experiments with four to five mice per group. (**H**) Immunoblots of anti-Myc precipitates from 293T cells cotransfected with Myc-tagged RORγt and HA-tagged WT or mutant IKKα^{Y580C}. Results are representative of two experiments. Bars represent means ± SEM. *$P < 0.05$, **$P < 0.01$, ***$P \leq 0.001$ by two-tailed Student's *t* test.

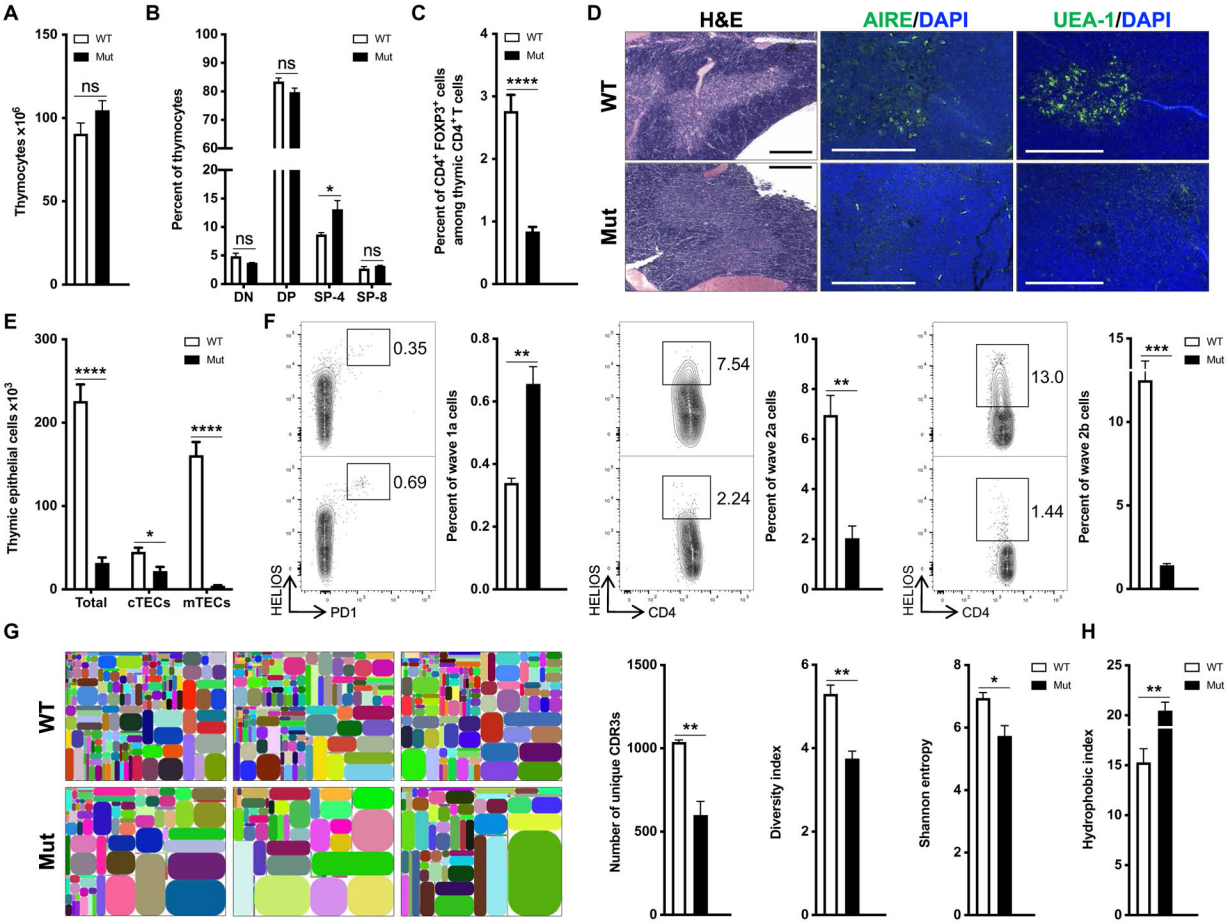

Fig. 7. IKKα$^{Y580C/Y580C}$ mice have abolished mTEC development, decreased thymic T$_{regs}$, and a restricted TCRVβ repertoire.

(**A**) Number of viable thymocytes in 6- to 8-week-old mutant mice and WT controls (n = 5 per genotype). (**B**) Distribution of DN, DP, CD4SP (SP-4), and CD8SP (SP-8) thymocyte subsets in mutant mice and WT controls (n = 5 per genotype). (**C**) Percent of thymic CD4$^+$FOXP3$^+$ T$_{regs}$ among CD4-SP cells in mutants and WT controls (n = 5 per genotype). (**D**) H&E staining (left) and immunofluorescence staining of AIRE or UEA-1 with 4′,6-diamidino-2-phenylindole (DAPI) in WT and mutant thymus. Scale bars, 275 μm (H&E) and 75 μm (IF, immunofluorescence). Similar results were obtained in three mice per genotype. (**E**) Number of CD45$^-$ClassII$^+$EpCAM1$^+$ total TECs, Ly51^{hi}UEA-1^{low} cTECs, and Ly51^{low}UEA-1^{hi} mTECs in the thymus of mutant mice and WT controls (n = 5 per genotype). (**F**) Representative FACS plots and distribution of thymocytes undergoing negative selection in waves 1a, 2a, and 2b (left, middle, and right, respectively) in mutants and WT controls (n = 3 per genotype). (**G**) Representative tree maps of WT and mutant CDR3s, number of unique CDR3s, diversity index, and Shannon entropy in sorted CD4$^+$CD8$^-$TCRβ^{hi}CCR7$^+$MHCI$^+$CD69$^-$CD25$^-$ M2 thymocytes (n = 6 per genotype). (**H**) Hydrophobicity index of CDR3 P6-P7 doublets in M2 thymocytes from mutants and controls (n = 6 per genotype). Columns and bars in (A) to (C) and (E) to (H) represent mean and SEM. *$P \leq 0.05$, **$P \leq 0.01$, ***$P \leq 0.001$, and ****$P \leq 0.0001$ by two-tailed Student's t test.

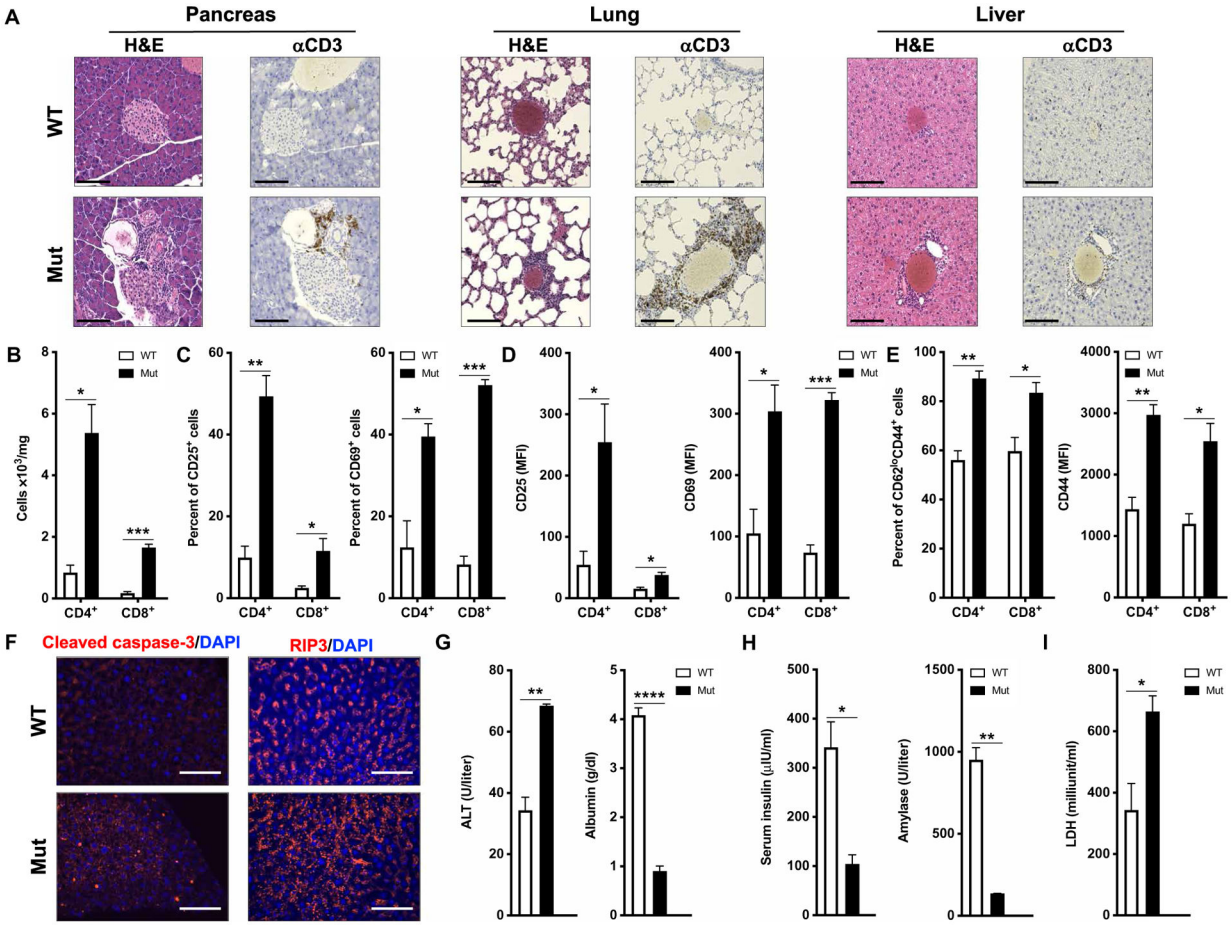

Fig. 8. Infiltration by activated T cells and organ damage in IKKα$^{Y580C/Y580C}$ mice.

(**A**) Representative H&E staining and staining for CD3 of pancreas lung and liver of 26-week-old mutant mice and WT controls. Scale bars, 125 μm. Similar results were obtained with six mice per genotype. (**B** to **D**) Number of $CD4^+$ and $CD8^+$ T cells (B) and percentage of $CD25^+$ and $CD69^+$ cells (C) and mean fluorescence intensity (MFI) of CD25 and CD69 expression (D) in $CD4^+$ and $CD8^+$ T cells isolated from the livers of 26-week-old mutants and WT controls ($n = 3$ per genotype). (**E**) Percentage of $CD62L^{low}CD44^+$ cells and MFI of CD44 expression in $CD4^+$ and $CD8^+$ T cells isolated from livers of 26-week-old mutant mice and WT controls ($n = 3$ per genotype). (**F**) Immunofluorescence staining for cleaved caspase-3 and RIP3 in liver sections from 26-week-old mutant mice and WT controls. Scale bars, 75 μm. Similar results were obtained with three mice per genotype. (**G** to **I**) Serum levels of ALT and albumin (G), insulin and amylase (H), and LDH (I) in 26-week-old mutant mice and WT controls ($n = 3$ per genotype). Columns and bars in (B) to (E) and (G) to (I) represent mean and SEM. $*P \leq 0.05$, $**P \leq 0.01$, $***P \leq 0.001$, and $****P \leq 0.0001$ by two-tailed Student's *t* test.

Table 1.

Hematologic and immunologic profile of the patient's blood.

Abnormal values are indicated using bolding. Values of CBC, lymphocyte subsets, and immunoglobulins shown between parentheses represent the normal range for age. Values of T cell proliferation shown between parentheses represent the mean of two HCs studied the same day as the patient. WBCs, white blood cells; N.D., not done; PHA, phytohemagglutinin.

Age at evaluation	**2 years**	**16 years**
CBC (complete blood count)		
Hemoglobin (g/liter)	11.2 (10.5–14.5)	**9.2** (11.3–13.4)
Hematocrit (%)	34.2 (32–42)	**29.1** (32.1–38.7)
Platelets (cells/μl)	325,000 (190,000–365,000)	222,000 (150,000–400,000)
WBCs (cells/μl)	10,400 (6000–10,800)	6110 (4400–8100)
Monocytes (cells/μl)	676 (240–920)	977 (200–1000)
Neutrophils (cells/μl)	3660 (2,016–8,370)	4099 (1500–8000)
Lymphocytes (cells/μl)	5730 (660–6372)	**850** (1400–3300)
Lymphocyte subsets		
$CD3^+$ (cells/μl)	4985 (2100–6200)	**400** (1000–2200)
$CD3^+CD4^+$ (cells/μl)	3689 (1300–3400)	**179** (530–1300)
Naive ($CD45RA^+CCR7^+$) (%)	N.D.	45.5 (21–61.4)
Central Memory ($CD45RA^-CCR7^+$) (%)	N.D.	33.7 (26.8–62.1)
Effector Memory ($CD45RA^-CCR7^-$) (%)	N.D.	20 (7.6–25.1)
TEMRA ($CD45RA^+CCR7^-$)(%)	N.D.	0.7 (0.7–6.6)
$CD3^+CD8^+$ (cells/ml)	798 (620–2000)	**144** (330–920)
Naive ($CD45RA^+CCR7^+$) (%)	N.D.	67.5 (26.7–72.9)
Central Memory ($CD45RA^-CCR7^+$) (%)	N.D.	4.1 (3.7–23.2)
Effector Memory ($CD45RA^-CCR7^-$) (%)	N.D.	21.4 (16.8–54.6)
TEMRA ($CD45RA^+CCR7^-$)(%)	N.D.	7 (3.9–72.0)
TCRγδ (%)	N.D.	2.1 (0.5–21.5)
$CD19^+$ (cells/μl)	**229** (610–2600)	**12** (110–570)
Naive ($IgM^+IgD^+CD27^-$) (%)	N.D.	**94.7** (61.6–87.4)

Age at evaluation	**2 years**	**16 years**
$CD19^{hi}CD21^{lo}$ (%)	N.D.	1.9 (1.1–10.0)
Switched memory ($IgD^{-}CD27^{+}$) (%)	N.D.	**0** (8.3–27.8)
IgM memory ($IgD^{+}CD27^{+}$) (%)	N.D.	**1.2** (3.5–24.1)
Terminally differentiated ($CD38^{hi}CD27^{hi}CD21^{lo}$)	N.D.	**0** (0.16–8.70)
Plasma cells ($CD38^{hi}CD20^{-}CD138^{+}$) (%)	N.D.	**0** (0.1–2.4)
$CD3^{-}CD56^{+}$ (cells/ml)	458 (180–920)	**25** (70–480)
$CD56^{bright}$ (%)	N.D.	**25** (4–8)
Immunoglobulins (mg/dl)		**On IVIG**
IgG	**89** (464–1051)	872 (487–1327)
IgA	<**5** (14–153)	<**2** (60–337)
IgM	**17** (48–168)	97 (49–286)
Proliferation (^{3}H-thymidine counts per min)		
Anti-CD3 mAb	97,000 (98,000)	N.D.
PHA	90,000 (52,000)	N.D.